International Journal of Nanomedicine

Dovepress
Taylor & Francis Group

Open Access Full Text Article

ORIGINAL RESEARCH

Self-Assembled Safflower Polysaccharide Nanoparticles as a Targeted Drug Delivery System for Enhanced Therapy of Hepatocellular Carcinoma

Haotian Bai[1,*], Jing Yang[2,*], Junhao Zhang[1], Rui Wang[1,3]

[1]College of Pharmacy, Heilongjiang University of Chinese Medicine, Harbin, Heilongjiang, 150040, People's Republic of China; [2]College of Basic Medical Science, Heilongjiang University of Chinese Medicine, Harbin, Heilongjiang, 150040, People's Republic of China; [3]Key Laboratory of Basic and Application Research of Beiyao, Heilongjiang University of Chinese Medicine, Ministry of Education, Harbin, Heilongjiang, 150040, People's Republic of China

*These authors contributed equally to this work

Correspondence: Rui Wang, College of Pharmacy, Heilongjiang University of Chinese Medicine, 24 Heping Road, Xiangfang District, Harbin, Heilongjiang, 150040, People's Republic of China, Tel +8613101669321, Fax +451 87266893, Email wrdx@sina.com

Purpose: Bone morphogenetic protein 7 (BMP7) plays a crucial role in the pathogenesis of hepatocellular carcinoma (HCC). Traditional therapies have severe side effects and cannot achieve the desired therapeutic effect. Delivery of small interfering RNA targeting BMP7 (siBMP7) can specifically down-regulate the expression of BMP7 and induce apoptosis of cancer cells, thereby achieving the effect of gene therapy. We aimed to use cationic safflower polysaccharide (SPS) as the basic carrier, and encapsulate it with synthetic hyaluronic acid (HA) and folic acid (FA) polymer to form a dual-targeting nano-carrier. After encapsulating siBMP7, we obtain dual-targeted self-assembled nanoparticles (NPs). This not only improves the delivery efficiency, maintains stability in the blood circulation, and enhances accumulation in the tumor site, but also achieves the effect of gene therapy for HCC.

Methods: We identified SPS, and then prepared and characterized the self-assembled NPs modified with polyethyleneimine (PEI), which can target the HA receptors and FA receptors on the surface of SMMC-7721 cells and deliver siBMP7 to hepatoma cells and induce cell apoptosis. The temperature stability, serum stability, cytotoxicity, buffering capacity, hemolytic properties, release behavior, uptake ability, and gene silencing effect of the NPs were evaluated in vitro. Further evaluation of their in vivo distribution, therapeutic effect, and safety was conducted in a nude rats model.

Results: The HA-FA polymer is light yellow and has strong water solubility. The blank NPs and self-assembled NPs have uniform particle size, physical stability, and stable release ability. HFSPNPs showed strong uptake ability and apoptotic effect in SMMC-7721 cells and LO2 cells. HFSPNPs could relatively effectively accumulate in the liver of rats and down-regulate the expression of BMP7 to induce apoptosis of hepatoma cells. Pathological analysis showed that the safety of HFSPNPs is better.

Conclusion: HFSPNPs have better tumor targeting properties, enabling siBMP7 to accumulate more in the tumor tissue and be released, thereby promoting apoptosis of hepatoma cells. This indicates that their potential for treating HCC is equivalent to that of gene therapy. This study highlights the potential of cationic SPS as a drug delivery material.

Keywords: dual-target, safflower polysaccharide, hepatocellular carcinoma, self-assembled nanoparticles

Introduction

Hepatocellular carcinoma (HCC) is one of the most prevalent malignancies and the second leading cause of cancer-related mortality.[1] Traditional treatments such as chemotherapy and surgery often come with significant side effects and suboptimal outcomes. In recent years, RNA interference (RNAi) technology has emerged as a promising gene interference technique and a novel therapeutic approach for cancer, complementing conventional treatments like surgery, chemotherapy, and radiation therapy. The advantages of RNAi technology in the treatment of HCC include strong selectivity, high specificity, rapid action, and effective gene silencing. This technology could be utilized to reduce the expression of critical oncogenes and key signaling pathway molecules in tumor cells, thereby inhibiting tumor growth.[2] Consequently, selecting an effective gene vector for targeted

Received: 3 June 2025
Accepted: 30 September 2025
Published: 5 November 2025

Graphical Abstract

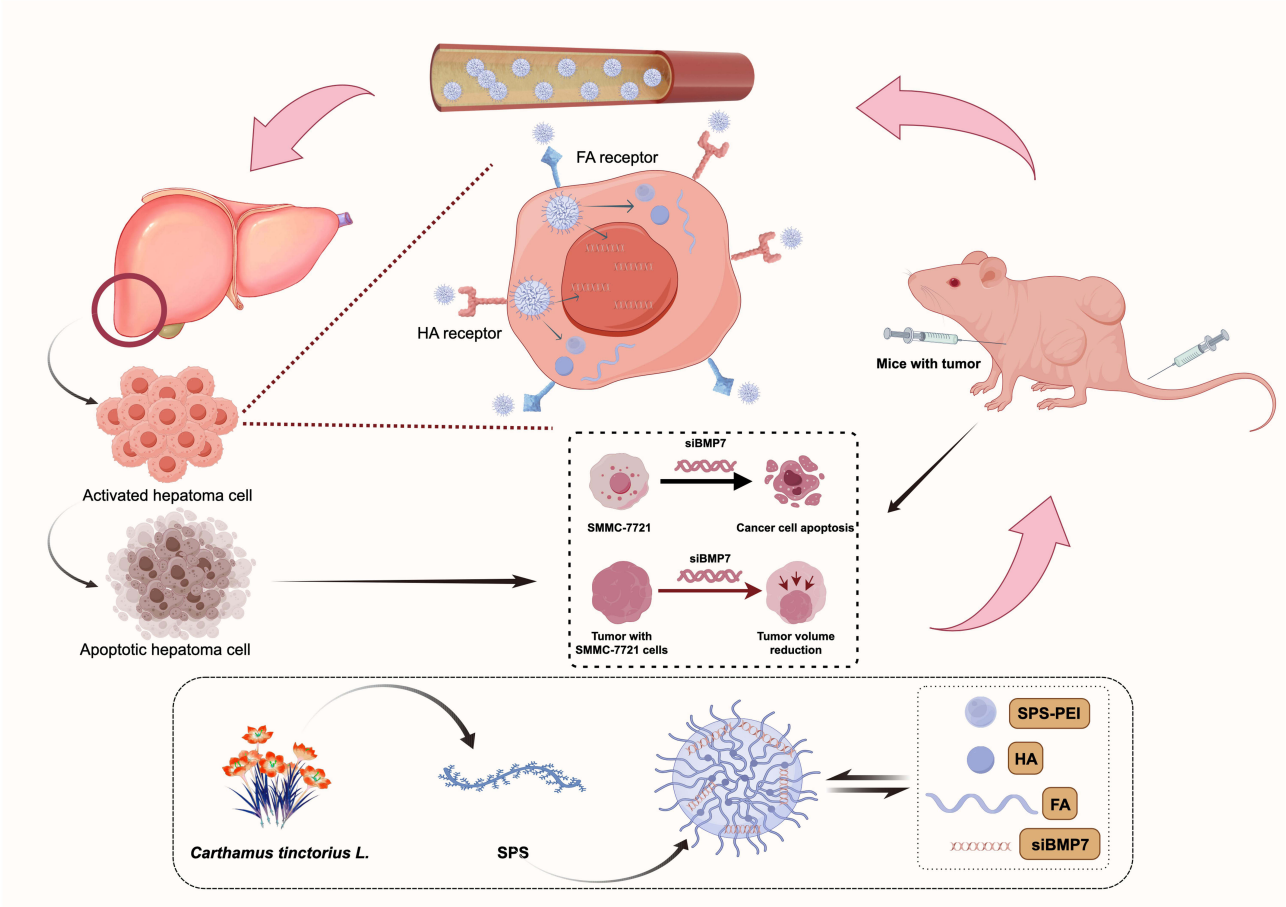

RNA delivery has become a significant challenge for RNAi technology. Interest in natural polysaccharides as safe, effective, and low-toxicity gene carriers has been steadily increasing among researchers. These polysaccharides are gaining attention in the field of biological materials due to their high non-toxicity, excellent biocompatibility, and biodegradability.[3] Recently, the research group successfully extracted Safflower polysaccharide (SPS) from Compositae *Carthamus tinctorius* L. As a natural polysaccharide, SPS possesses anti-tumor, anti-oxidative, and immune-enhancing properties, and contains active hydroxyl (-OH). Chemical modification of these -OH groups can facilitate the synthesis of SPS with various biological effects. Polyethyleneimine (PEI) is a well-known transfection agent characterized by a high transfection rate, good biocompatibility, and low toxicity. Given their complementary advantages, researchers have employed these two materials to modify the natural polysaccharide, using PEI as the gene carrier.[4] Cationic polysaccharide carriers possess distinct advantages over other cationic polymers, including low cytotoxicity and immunogenicity, good biodegradability, and high water solubility.[5] Following the selection of appropriate vectors, targeted delivery to diseased organs has emerged as a pressing issue requiring resolution. The receptor-mediated targeted gene delivery system represents the most advanced cell-specific vector system, characterized by high specificity and affinity, significantly enhancing drug delivery efficiency.[6,7] Commonly utilized specific receptors include hyaluronic acid (HA), folic acid (FA), integrins, and galactose receptors. As an innovative targeted drug delivery strategy, dual-receptor-mediated approaches can more effectively direct nanoparticles (NPs) to specific sites. Consequently, dual receptor-mediated targeting strategies have been increasingly adopted in drug delivery systems in recent years.[8] Bone morphogenetic proteins (BMPs) are a group of functional proteins that play crucial roles in biological processes regulating cell proliferation, differentiation, and apoptosis. BMP expression is integral to embryo and organ formation, as well as the development of tumor

Table 1 Sequence of siRNA

Name	Upstream Primers	Downstream Primers
siBMP7	CCG UCC UCU ACU UCG AUG AdTdT	UCA UCG AAG UAG AGG ACG GdTdT
siRNA/siRNA^{FAM}	UUC UCC GAA CGU GUC ACG UdTdT	ACG UGA CAC GUU CGG AGA AdTdT
β-actin	CTC CAT CCT GGC CTC GCT GT	GCT GTC ACC TTC ACC GTT C

diseases. A growing body of research indicates that bone morphogenetic protein 7 (BMP7) is significantly expressed in various epithelial tumors, including breast cancer, primary melanoma, prostate cancer, and colorectal cancer.[9–11] However, the relationship between BMP7 gene alterations and the malignant biological characteristics of hepatocellular carcinomas—such as differentiation degree, proliferation, invasion, metastasis, and recurrence—remains underexplored in the international literature.

Based on the aforementioned studies, SPS-PEI was chosen as the primary gene carrier for this research, with siRNA bound via electrostatic adsorption. HA and FA were covalently linked to form a polymer through an esterification reaction, which was subsequently coated with SPS-PEI to enhance delivery efficiency. This approach not only shields the positive charge to minimize cytotoxicity but also targets both FA and HA receptors on the surface of SMMC-7721 cells, thereby constructing a dual-targeted nano gene vector.

Materials and Methods

The dried tubular flower of *Carthamus tinctorius* L. was collected and identified by Prof. Rui Wang (College of Pharmacy, Heilongjiang University of Chinese Medicine) at the Medical Botany Center of Heilongjiang University of Chinese Medicine, where a voucher specimen (No. 20250517) has been deposited. Detailed information of sequence of siRNA is shown in Table 1. Details on the key reagents and instrumentation are available in the Supplementary Tables S1 and S2.

Separation and Purification of SPS

Unrefined SPS was extracted following the methodology outlined in a previous study.[12] The specific operational details are provided in the Supplementary Data. The phenol-sulfuric acid method was employed for colorimetric analysis, with absorbance measured at 490 nm. Polysaccharide samples exhibiting identical elution peaks were collected for further analysis. The elution curve was plotted with the tube number as the abscissa (X) and absorbance (A) as the ordinate (Y). The components were separated and purified using Sephadex G-100, and subsequently prepared into a solution at a concentration of 1 mg/mL after undergoing dialysis, concentration, and freeze-drying. The resulting solution was then scanned with a UV spectrophotometer (Shimadzu) across a wavelength range of 200 to 800 nm, with ultrapure water serving as the blank control. Characteristic absorption peaks corresponding to nucleic acids (260 nm) and proteins (280 nm) were detected (see Supplementary Figure S1). The separation and purification process is illustrated in Figure 1.

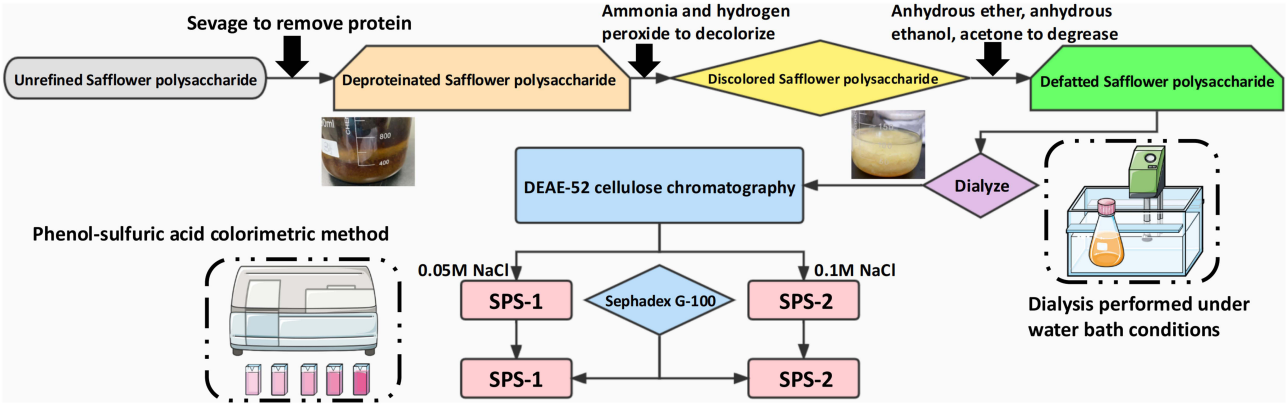

Figure 1 Separation and purification process of safflower polysaccharide.

https://doi.org/10.2147/IJN.S544439

Structural Identification of SPS

Total Carbohydrate and Uronic Acids Determination

Glucose and glucuronic acid control solutions with concentrations of 20/40/60/80/100 μg/mL were prepared. Standard curves (Supplementary Figure S2) were drawn using glucose concentration as abscissa (*X*) and absorbance as ordinate (*Y*). Total polysaccharides and uronic acids were determined using sulfuric acid-anthracone and sulfuric acid-carbazole method.

Relative Molecular Mass

A reference solution of dexglucoside series was prepared at a concentration of 1 mg/mL, from which 500 μL aliquots were sequentially taken. Three replicates of each sample were analyzed in parallel, and the retention times of their elution peaks were recorded under established chromatographic conditions. The standard curve (Supplementary Figure S3) was constructed using the logarithm of the molecular weight (MW) of the reference substance against its corresponding retention time (tR), resulting in the linear regression equation lgMW = a + btR. The polysaccharides SPS-1 and SPS-2 (50 μL each), prepared as previously described, were analyzed using the same method, and the retention time (tR) of the polysaccharides was recorded. The weight average molecular weight (Mw), number average molecular weight (Mn), and polydispersity index (D) of the polysaccharides were calculated based on the established standard curve.

Monosaccharide Composition

The monosaccharide components were analyzed using pre-column derivatization high performance liquid chromatography (HPLC) (Shimadzu). The purified SPS-1 and SPS-2 (50 mg) were respectively weighed in a hydrolysis tube, and ultrapure water (3 mL) and 4 mol/L trifluoroacetic acid (1 mL) were added. Under conditions of nitrogen protection, the solution was hydrolyzed at 110°C for 2 h and then cooled to room temperature. Then solution (0.1 mL) was placed in a centrifuge tube, and vacuum dried at 60°C (2 h). The standard monosaccharides were obtained by sequentially adding 5 mg of D-glucose (D-glu), D-galactose (D-gal), D-galacturonic acid (D-gal-A), D-xylose (D-xyl), D-mannose (D-man), L-rhamnose (L-rha), and L-arabinose (L-ara) to a volumetric flask. In addition, the standard monosaccharide solution (500 μL) (200-059-4; Merck Bio-Science) and 2 hydrolyzed polysaccharide samples were placed in a centrifuge tube. Then 0.3 mol/L NaOH (0.05 mL) and 1-phenyl-3-methyl-5-pyrazolone methanol solution (PMP) (0.05 mL) were added to each tube. The reaction was performed in a water bath at 70°C under nitrogen protection and cooled to room temperature (1 h). Then 0.3 mol/L HCl (0.5 mL), H_2O (0.75 mL), and chloroform (1.5 mL) were added for extraction. The chloroform layer was discarded and extracted three times. The water layer was combined with PMP-derived products on the upper layer and filtered by means of filter membranes (0.45 μm). The samples were directly injected for gas chromatography (GC) analysis.

The monosaccharide components were analyzed using pre-column derivatization high-performance liquid chromatography (HPLC) (Shimadzu). A total of 50 mg of purified SPS-1 and SPS-2 were weighed into separate hydrolysis tubes, to which 3 mL of ultrapure water and 1 mL of 4 mol/L trifluoroacetic acid were added. Under nitrogen protection, the solution was hydrolyzed at 110°C for 2 hours and subsequently cooled to room temperature. Following this, 0.1 mL of the solution was transferred to a centrifuge tube and vacuum-dried at 60°C for 2 h. Standard monosaccharides were prepared by sequentially adding 5 mg each of D-glucose (D-glu), D-galactose (D-gal), D-galacturonic acid (D-gal-A), D-xylose (D-xyl), D-mannose (D-man), L-rhamnose (L-rha), and L-arabinose (L-ara) into a volumetric flask. Additionally, 500 μL of the standard monosaccharide solution (200-059-4; Merck Bio-Science) and two hydrolyzed polysaccharide samples were placed in a centrifuge tube. Subsequently, 0.3 mol/L NaOH and 0.05 mL of 1-phenyl-3-methyl-5-pyrazolone (PMP) methanol solution (0.05 mL each) were added to each tube. The reaction was conducted in a water bath at 70°C under nitrogen protection and cooled to room temperature after 1 h. Following this, 0.3 mol/L HCl (0.5 mL), H_2O (0.75 mL), and chloroform (1.5 mL) were added for extraction. The chloroform layer was discarded after three extractions. The water layer containing the PMP-derived products was combined with the upper layer and filtered using 0.45 μm filter membranes. The samples were then directly injected for gas chromatography (GC) analysis.

FT-IR Analysis

SPS-1 and SPS-2 (3 mg) were ground and compressed using KBr. A total of 24 scans were performed within the 4000~400 cm^{-1} range.

^{1}H-NMR Analysis

Prior to NMR analysis, over-dried polysaccharide (30 mg) was dissolved in of 99.97% D_2O (0.5 mL) for 6 h after being repeatedly freeze-dried in D_2O to exchange deuterium. On a Bruker AV-500 spectrometer (Bruker), the ^{1}H- was acquired at 30°C at 500 MHz for ^{1}H. The acquisition time (AT=0.5 s), sweep width (SWH=20,000 Hz), relaxation delay (d1=10 s), and 90° pulse time (p1=2.5 μs) were the parameters that were specified for the ^{1}H-NMR spectra. The recordings were made with a relaxation delay of 1.5 s. Chemical shifts are measured in parts per million (ppm) and are calibrated internally using acetone, which has a δ31.21 ppm for carbon and a δ2.19 ppm for hydrogen. The TopSpinTM3.5 program from Bruker was used to evaluate the data.

Congo Red Analysis

After thoroughly mixing Congo red solution (1.5 mL) with polysaccharide solution (1 mL) and ultrapure water (0.5 mL), the mixture was split into 10 equal portions. Concurrently, the aqueous solution containing polysaccharides was converted to an aqueous solution and designated as the blank control group. For around 10 min, the solution was incubated at room temperature. UV scanning was carried out at a wavelength of 200~600 nm.

Periodic Acid Oxidation Analysis

A consistent volume of 15 mmol/L potassium periodate (KIO_4) original solution was created, and its concentration was diluted to 10/15/30/45/60 μmol/L KIO_4 solution. The UV absorbance was measured at 223 nm. KIO_4 concentration was represented by the x-coordinate (X) on the standard curve (Supplementary Figure S4), and absorbance value by the y-coordinate (Y). To stop the reaction at room temperature, SPS (5 mg) and KIO_4 solution (10 mL) was added. Subsequently, solution (100 μL) was taken at 0/4/8/12/24/48 h. With the use of KIO_4, the consumption of KIO_4 could be calculated. In order to use up the extra KIO_4, glycol (1 mL) was added last, shaking for 10 min. To ascertain the amount of formic acid produced, the previously described oxidized solution was added along with 2 drops of phenolphthalein indicator, and the mixture was titrated with 0.01 mol/L NaOH.

Synthesis and Characterization of the SPS-PEI Polymer

As per an earlier study, the SPS was isolated from safflower and refined. An esterification reaction could bond PEI to SPS.[13] The specific operational details are presented in Supplementary Data.

Using DMSO d6 as the solvent at 400 MHz, FT-IR spectroscopy Nicolet 170SX and ^{1}H-NMR spectrometry were used to determine the chemical structures of SPS and SPS-PEI polymer. By employing fluorescence spectroscopy with pyrene as a hydrophobic probe, the critical aggregation concentration (CAC) of the SPS-PEI conjugate was used to measure its self-aggregation characteristic. With an emission wavelength of 372 nm, the fluorescence excitation spectra were obtained using a F7000 fluorescence spectrometer (Hitachi) operating in the 300~360 nm range. For the purpose of measuring the intensity ratio, the fluorescence intensities at 339 and 335 nm (I_{339} and I_{335}) were noted. The monosaccharide composition of the SPS-PEI conjugate was analyzed using the same method as that for SPS. Thermogravimetric analysis (TGA) of SPS-PEI was conducted using a thermogravimetric analyzer (Hitachi). The sample was sealed under a nitrogen flow at a rate of 100 mL/min, with the temperature range set from 40°C to 600°C and the heating rate at 10°C/min. In order to investigate the morphology of SPS conjugate in more detail, the sample solution was placed onto copper grids covered with carbon, negatively stained for 2.5 min with a solution of 1% phosphotungstic acid, and allowed to air dry at room temperature. An H-7000FA Transmission Electron Microscope (Olympus) was used to image ultrastructure of NPs. Zeta potentials of SPS-PEI polymer were dissolved in an appropriate phosphate buffer solution (PBS; PH=7.4) measured using a Nano90 Malvin Laser (Malvin) at 25°C and a 90° scattering angle using dynamic light scattering (DLS).

Synthesis and Characterization of HA-FA Polymer and NPs

An esterification reaction could bind HA to FA.[14] The specific operational details are provided in the Supplementary Data. The FT-IR and ^{1}H-NMR analysis procedure used for HA-FA was the same as that used for SPS. HA-SPS-PEI and HA-FA-SPS-PEI polymers were produced using the magnetic-stirring technique depicted in Figure 2. In summary, polymers was dissolved in DMSO (1 mL) being continuously stirred at room temperature (1000 rpm) and dialyzed against ultrapure water for a day.

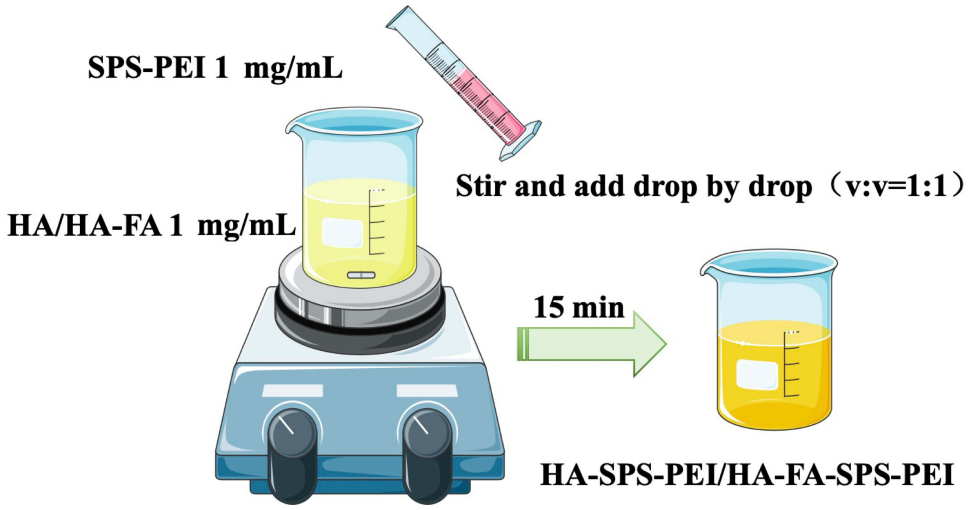

Figure 2 The production process of HA-SPS-PEI and HA-FA-SPS-PEI.
Abbreviations: SPS, safflower polysaccharide; PEI, polyethyleneimine; FA, Folic acid; HA, hyaluronic acid.

A well-dispersed nanoparticle solution was then achieved by sonicating the mixture for 3 min. SPS-PEI, HA-SPS-PEI, and HA-FA-SPS-PEI self-assembled nanoparticles (SPNPs, HSPNPs, and HFSPNPs) were prepared through the dialysis-sonication approach. The positively charged NPs were adsorbed by electrostatic attraction onto the negatively charged free siRNA (scrambled siRNA), siRNA targeting BMP7 (siBMP7) or fluorescein-labeled siRNA ($siRNA^{FAM}$). After uniformly mixing the siRNA with the polymer in a certain proportion and leaving it at room temperature for 15 min, siRNA-loaded NPs (siRNA/SPNPs, siRNA/HSPNPs, and siRNA/HFSPNPs) were obtained after lyophilization. (Both $siRNA^{FAM}$-loaded NPs and siBMP7-loaded NPs were obtained using the aforementioned methods).

Zeta potentials of siRNA-loaded NPs solutions were dissolved in an appropriate phosphate buffer solution (PBS; PH=7.4) measured using a Nano90 Malvin Laser (Malvin) at 25 °C and a 90° scattering angle using dynamic light scattering (DLS). In order to investigate the morphology of the NPs in more detail, the sample solutions (1 mg/mL) were placed onto copper grids covered with carbon, negatively stained for 2.5 min with a solution of 1% phosphotungstic acid, and allowed to air dry at room temperature. An H-7000FA Transmission Electron Microscope (Olympus) was used to image ultrastructure of NPs.

Cell Culture

SMMC-7721 hepatoma cells and LO2 human normal liver cells were cultured in SMMC-7721/LO2 cell-specific medium (CM-0113/CM-0022; Pricella Biotechnology) containing 10% Fetal Bovine Serum (FBS) at 37°C/5% CO_2.

Biocompatibility of Blank NPs

Indicators for assessing the biocompatibility of the SPNPs, HSPNPs, and HFSPNPs included serum stability, cytotoxicity, buffer capacity and hemolytic properties.

For the serum stability test, 100 μL of FBS was combined with 0.9% NaCl (negative group) or the same volume of SPNPs, HSPNPs, and HFSPNPs solution at different concentrations. A UV-Vis spectrophotometer was used to measure the absorbance of each group at 630 nm at 0/2/6/12/18/ 24 h after incubation in a water bath at 37°C away from light. By computing the absorbance ratio between the samples and the negative group at each time point, the relative turbidity was determined.

After being seeded in 96-well plates (3×10^3 cells/well), LO2 and SMMC-7721 cells were cultivated for a whole night. Upon being treated for 96 h with 0/1/10/20/40/80/160 μg/mL of SPNPs, HSPNPs, and HFSPNPs, of MTT (20 μL; 5 mg/mL) was added to each well, and the mixture was incubated for an extra at 37°C (4 h). Following the formation of formazan crystals, DMSO (150 μL) was added, and a microplate reader was used to measure the absorbance at 570 nm.

Wells devoid of any cells served as the blank, and the untreated cells served as the control. Five analyses were conducted on each sample at each concentration. The following formula was used to determine.

$$\text{cell viability}\,(\%) = \frac{A_{570\,(\text{treated})} - A_0}{A_{570\,(\text{untreated})} - A_0}$$

where $A_{570(\text{treated})}$ is the absorbance of cells treated with samples, $A_{570(\text{untreated})}$ is the absorbance value of the untreated cells, and A_0 is the absorbance value of the blank medium.

The buffer capacity of the SPNPs, HSPNPs, and HFSPNPs was investigated via acid-base titration. Following the dispersion of SPNPs, HSPNPs, or HFSPNPs (0.2 mg/mL) in the aqueous NaCl solution (0.15 mol/mL), an aqueous NaOH solution (0.1 mol/mL) was added until the pH reached 10. Then, a solution of 0.1 mol/mL HCl (3–5 μL) was added. The pH of the mixture was determined using a microprocessor pH meter following each addition of the HCl solution. NaCl solution as the negative control (0.15 mol/mL).

To investigate the hemolytic characteristics of NPs, the hemolysis experiment was conducted. The flask was filled with around SD Rat heart blood (5 mL). The flask was filled with around 10 times as much sterile 0.9% NaCl saltwater, shaken, and centrifuged for ten minutes at 1500 rpm. The sedimented red blood cells (RBC) were rinsed with saline two or three times until the supernatant was clear after the supernatant was removed. RBC and sterile saline were combined to create 2% of the RBC solution. 2% RBC were added to sterile saline, ultrapure water, and different NPs (0.1 mg/mL SPNPs, HSPNPs, or HFSPNPs) and placed into five tubes. The tubes were then left to incubate at ambient temperature. The hemolysis phenomenon was observed at different time points. Tubes holding sterile saline and ultrapure water were divided into negative and positive groups, respectively. UV-vis spectrophotometry was used to determine the OD values and hemolysis rates (HRs) of each group's supernatant using the following formula:

$$\text{HR} = \frac{OD_0 - OD_1}{OD_2 - OD_1} \times 100\%;$$

OD_0, OD_1 and OD_2 represented the OD values of NPs, negative group and positive group.

Stability of siRNA-Loaded NPs

To investigate the stability of siRNA-loaded NPs during storage and physiological condition, take 1 mL of the siRNA/SPNPs, siRNA/HSPNPs, or siRNA/HFSPNPs (scrambled siRNA) solution, and disperse it in 10 mL of PBS (pH 7.4) or fetal bovine serum (FBS; 10%). Then store them respectively at 4/25/37°C. At different time points (day 0/7/14/21/28), the average size, zeta potential, and polydispersity index (PDI) of the NPs were monitored using a Nano 90 Malvin Laser (Malvin).

The stability of siRNA encapsulation efficiency was measured by a spectrofluorometer set (Shimadzu) at the same intervals over 28 days. The prepared siRNA-loaded NPs were ultra-centrifuged at 4°C, 12,000 rpm for 30 min. The fluorescence intensity value was then measured by adding Ribogreen fluorochrome (x200) and TBE solution. Then, the content of free $siRNA^{FAM}$ in the supernatant was measured and the $siRNA^{FAM}$ encapsulation efficiency (EE) was calculated as follows:

$$\text{EE}\,(\%) = \frac{C_{\text{total}} - C_{\text{free}}}{C_{\text{total}}}$$

Drug Release Study in vitro

Utilizing dynamic dialysis procedure in PBS (pH 7.4) containing 0.5% Tween 80 and 10% ethanol, the $siRNA^{FAM}$ release capacity from SPNPs, HSPNPs, and HFSPNPs was investigated.[15] In a nutshell, the release media (50 mL) were dialyzed against free siRNA and $siRNA^{FAM}$/SPNPs (1 mL), $siRNA^{FAM}$/HSPNPs, or $siRNA^{FAM}$/HFSPNPs (scrambled siRNA) solution at 37°C in a shaking incubator at 120 rpm. The release medium was swapped out on a regular basis for equivalent amounts of brand-new release medium. Every experiment was conducted in triplicate, and the amount of released siRNA was determined using a fluorescence spectrometer (Hitachi).

Cellular Uptake

In order to confirm that the NPs could target the liver, SPNPs, HSPNPs, and HFSPNPs were labeled with $siRNA^{FAM}$, a simulated fluorescent marker. LO2 cells and SMMC-7721 cells were seeded on coverslips in 24-well plates for the qualitative cellular uptake study. The cells were then separated into the following groups: free $siRNA^{FAM}$, $siRNA^{FAM}$/SPNPs, $siRNA^{FAM}$/HSPNPs, $siRNA^{FAM}$/HFSPNPs, and $siRNA^{FAM}$/HFSPNPs (scrambled $siRNA^{FAM}$) with the antagonist HA (or FA) (HA and FA pretreatment at a concentration of 1 mg/mL). The cells were exposed to new medium containing free $siRNA^{FAM}$ or $siRNA^{FAM}$ NPs ($siRNA^{FAM}$ concentration = 100 nM) for 1/2/4 h following 24 h of cell attachment. After discarding the media, their nuclei were then stained for 20 min with 4′,6-diamidino-2-phenylindole (DAPI) (AB2001; Aladdin Biochemical Technology) in order to identify them. A confocal laser scanning microscope (CLSM) (Zeiss) was used to take the pictures for the quantitative cellular uptake investigation. Following an incubation period (24 h), the cells were subjected to several $siRNA^{FAM}$ forms utilizing the identical procedure. As a negative control group, cells that were not given medication were employed. The cells were identified using flow cytometry after being resuspended in PBS solution (500 μL).

Gene Silencing

SMMC-7721 cells were cultivated in DMEM (2 mL) with 10% FBS for 24 h after being plated at a density of 4×10^4 cells per well in 6-well plates. The cells were allowed to incubate for 4 h before being incubated for a further 20 h with fresh medium after the medium was replaced with opti-MEM containing $siRNA^{FAM}$/HFSPNPs (1:1, 5:1, 10:1, and 20:1) (scrambled $siRNA^{FAM}$). The lysis buffer was used to extract the transfected cell proteins. Proteins were separated via gel electrophoresis after being put in equal amounts into the wells of a 10% SDS-PAGE gel. Upon transferring the proteins from the gel to the polyvinylidene difluoride membrane, the membranes were blocked with 5% BSA (1 h). The membranes underwent 16 h of incubation at 4°C with BMP7 antibody (1:1000) (A0155; Abways) and β-actin antibody (1:5000) (A0011; Abways), followed by secondary antibody treatment (1 h). Applying an enhanced ECL detection technique, the expression of BMP7 was identified. A Mini Chemi610 Imaging System (Sinsage) was used to identify the Western blot signals.

Acridine Orange (AO) Staining

Before inoculating coverslips with SMMC-7721 hepatoma cell suspensions, the coverslips were placed in 6-well plates. After division into control (PBS), HFSPNPs (only blank NPs dissolved in PBS), free $siRNA^{FAM}$, $siRNA^{FAM}$/SPNPs, $siRNA^{FAM}$/HSPNPs, $siRNA^{FAM}$/HFSPNPs groups (scrambled $siRNA^{FAM}$), the cells were incubated for 24 h, resuspended in a 10-fold diluted buffer solution. Working solution (10 μL), prepared by combining AO (A6073; Sangon Biology) in a 1:1 ratio, was added to the cell suspension (90 μL) in the dark (10 min). Apoptosis was examined using an IX85 inverted microscope (Olympus).

Experimental Animals

Male BALB/c nude mice (6-weeks old, 16~20 g) (accession number: 202409100) were procured from the Experimental Animal Center of Heilongjiang University of Chinese Medicine (animal certificate: SYXK [black] 2024-103). Mice were acclimated for 1 week prior to experimentation. All studies were approved by the Institutional Animal Care and Use Committee (IACUC) of Heilongjiang University of Chinese Medicine and were conducted in accordance with the National Laboratory Animal Management Regulations and the principles of experimental animal protection.

Distribution in vivo

SMMC-7721 cells were suspended in PBS at a density of 1×10^7 cells/mL. Male BALB/c nude mice were infected with cell solution (0.1 mL) in the axilla. In the study of in vivo biodistribution, when the tumor size was approximately (100 ±20) mm^3, Free siRNA, siRNA/SPNPs, siRNA/HSPNPs and siRNA/HFSPNPs (scrambled siRNA labeled with FITC; 250 μL) were injected into tumor-bearing mice via the tail vein. Images were captured on the IVIS imaging system at 1 h and 12 h after injection.

Body Mass and Tumor Status

In order to initiate a focused experimental inquiry in vivo, 5 groups (n=5) of mice were randomly assigned: 1. Control group (saline); 2. HFSPNPs (only blank NPs dissolved in saline); 3. Free siBMP7; 4. siBMP7/SPNPs; 5. siBMP7/HSPNPs; and 6. siBMP7/HFSPNPs. Every 2 days, an intravenous injection of either the standard saline or the various siBMP7 formulations (200 μL; equal to 0.33 mg/kg/day) was given into the tail 4 times in a row. Following the 4th dosage, the mice were put to sleep after an 8-hour fast (Figure 3). Body mass was quantified at 2-d intervals and tumor volume was weighed from the seventh day. Tumor weight was weighed when the tissue was removed.

Hematoxylin-Eosin (H&E) Staining

Primary organs and tumor tissues of mice were completely removed. For further H&E staining, all tissues were fixed in a 10% formalin solution and seen using a Leica DM2500 fluorescence microscope (Leica).

Western Blotting

RIPA buffer with PMSF (1 mM) and 1% protease and phosphatase inhibitors were used to lyse the frozen tumor samples. Incubation with the primary antibodies against BMP7 (1:1000) and β-actin (1:4000) was employed at 4°C overnight. The membranes were subsequently incubated with horseradish peroxidase-conjugated anti-rabbit IgG. Densitometry using ImageJ software was calculated for quantification, and the densitometry results were normalized relative to the β-actin bands.

Inflammatory Response

To further detect the immune response in vivo, blood was collected on the 1st and 3rd days after intravenous administration. Plasma was separated for the detection of the secretion levels of IL-1β, IL-6, and TNF-α by ELISA for cytokine analysis.

Safety Evaluation

For safety evaluation, the tumor tissues and major organs of mice were dissected and fixed in 4% paraformaldehyde at room temperature for 24 h. Sections were prepared by paraffin embedding and H&E staining and observed and photographed under a CKX41 Optical microscope (Olympus).

Statistical Analysis

All experimental data were performed at least in triplicate and expressed as mean ± standard deviation. Statistical comparisons between groups were carried out using a one-way analysis of variance followed by the Student's *t*-test. Values of $P<0.05$ were considered statistically significant.

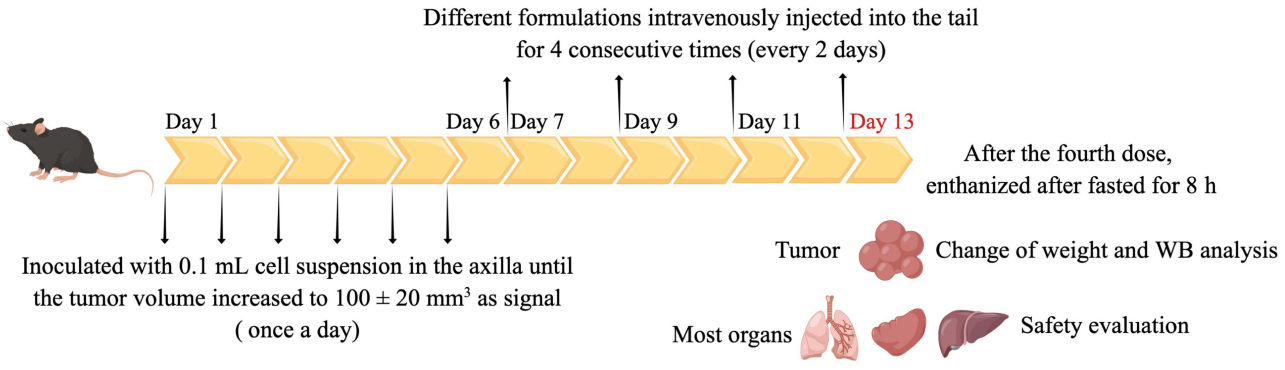

Figure 3 Overview of the tumor-bearing model. The mice were euthanized on Day 13.

https://doi.org/10.2147/IJN.S544439

Results

Separation, Purification and Component Identification of SPS

37.7 g of crude polysaccharide SPS (yield 7.54% of 500 g of dry material) was produced from dried safflower. SPS-1 (2.92 g, yielding 0.58% of 500 g dried safflower) and SPS-2 (1.72 g, yielding 0.34% of 500 g dried safflower) were obtained through purification on DEAE-cellulose (Figure 4A) and Sephadex G-100 chromatographic columns (Figure 4B and C). For the next physicochemical and animal tests, the peaks of SPS-1 (carbohydrate contents of 94.2%) and SPS-2 (carbohydrate contents of 92.1%) were collected.

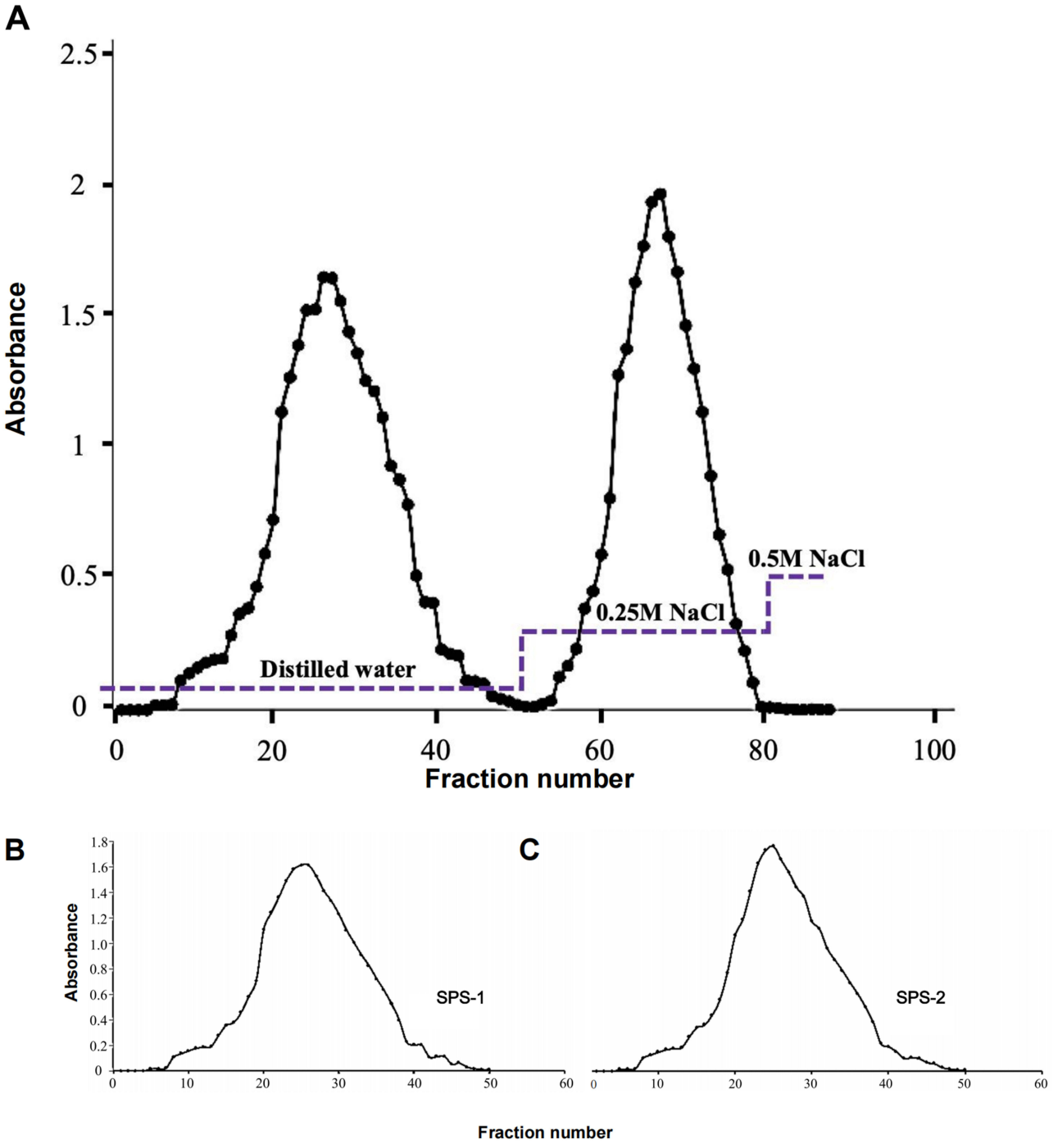

Figure 4 Elution curve of the crude polysaccharide obtained from safflower on a column of DEAE-cellulose (**A**). Elution curve of SPS-1 (**B**) and SPS-2 (**C**) on a column of SephadexG-100.

Abbreviation: SPS, safflower polysaccharide.

As shown in Figure 5A, Table 2 and Table 3, the derivatives of monosaccharide standard D-glucose (Glu), D-galactose (Gal), D-xylose (Xyl), D-galacuronic acid (Gala), D-mannose (Man), L-rhamnose (Rha) and L-arabinose (Ara) showed absorption peaks at about 26.025, 29.398, 30.700, 22.450, 12.759, 17.051 and 32.137min, respectively. Monosaccharide components of SPS-1 were respectively Man, Glu, Xyl, Ara, Gal, Rha, the mole ratio is: 5.36:8.72:4.61:1.96:19.36:4.52. The monosaccharide components of SPS-2 were Rha, Glu, Gal, Ara and Man with molar ratios of 3.00:7.12:5.88:1.16:4.02.

The molecular weight of polysaccharide chromatogram is shown in Figure 5B and Table 4. The larger the polydispersity, the wider the molecular weight distribution. Both SPS-1 and SPS-2 are polydisperse samples, that is, the sample is widely distributed. As shown in Figure 5C, the proton peak signal at δH4.69 ppm indicates that it belongs to the sub-peak signal of β-D-glu residue

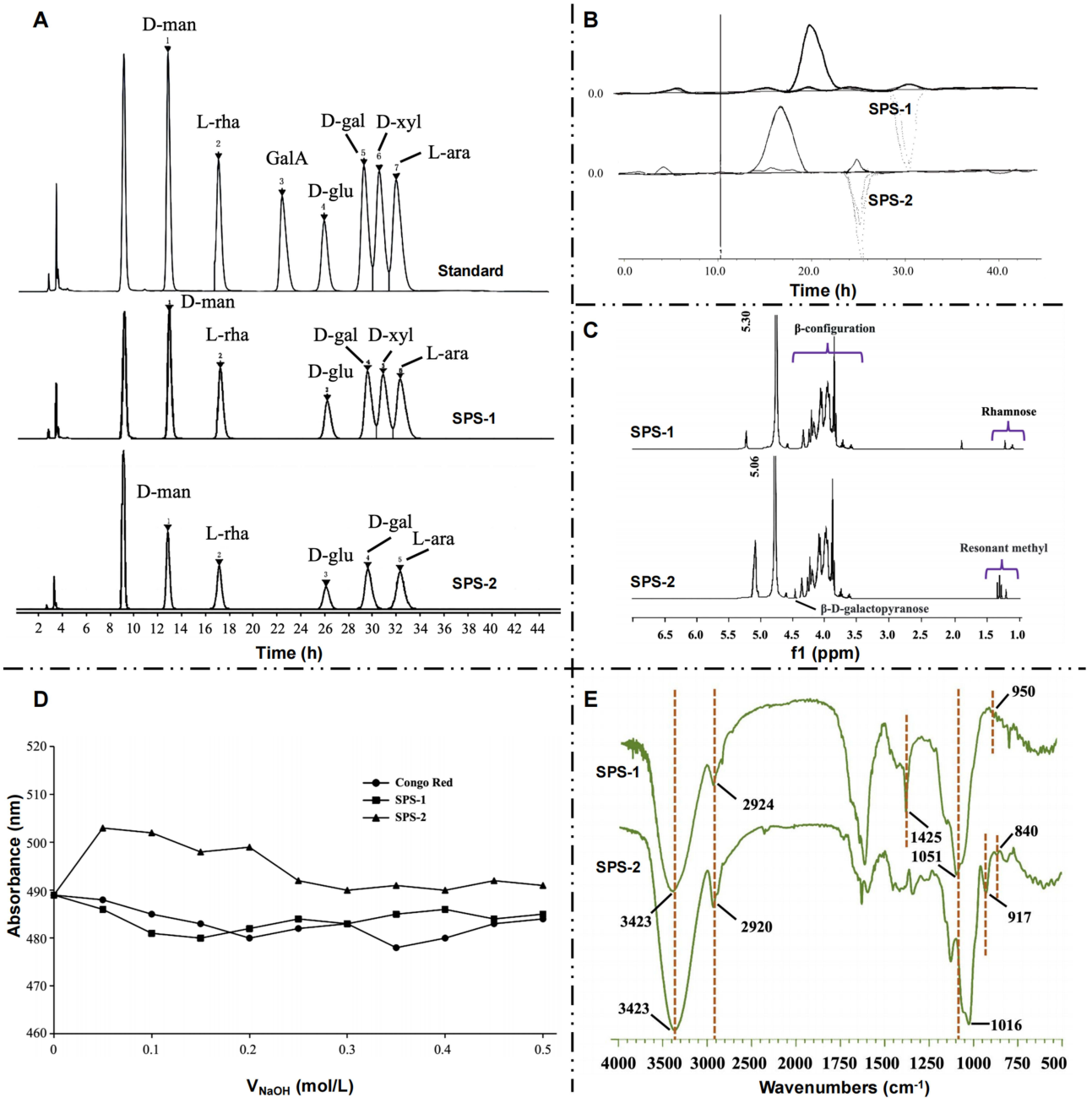

Figure 5 PMP derivatives of standard monosaccharides and the monosaccharide composition of SPS-1/2 by HPLC (**A**). Polysaccharide molecular weight (**B**), ^{1}H-NMR spectrum (**C**) Congo Red structure analysis (**D**) and FT-IR spectrum (**E**) of SPS-1/2. The numbers represent the wavelengths of the corresponding peaks.
Abbreviations: SPS, safflower polysaccharide; D-glu, D-glucose; D-gal, D-galactose; GalA, galacturonic acid; D-xyl, D-xylose; D-man, D-mannose; L-rha, L-rhamnose; L-ara, L-arabinose.

https://doi.org/10.2147/IJN.S544439

Table 2 Analysis of SPS-1 Monosaccharide Composition

Name	Retention Time (min)	Response Factor	Peak Area	Content (mg/L)
Man	12.832	155.140	10549.999	163.362
Rha	17.168	119.512	9808.048	137.762
Glu	26.124	169.428	21132.109	265.768
Gal	29.786	165.248	40087.860	590.054
Xyl	31.030	173.850	8488.045	140.503
Ara	32.424	182.093	5880.004	48.76

Abbreviations: Man, mannose; Rha, rhamnose; Glu, glucose; Gal, galactose; Xyl, xylose; Ara, arabinose.

Table 3 Analysis of SPS-2 Monosaccharide Composition

Name	Retention Time (min)	Response Factor	Peak Area	Content (mg/L)
Man	12.805	155.140	15285.930	168.530
Rha	17.114	119.512	11761.550	128.413
Glu	26.083	169.428	18316.426	209.085
Gal	29.585	165.248	16267.695	198.444
Ara	32.284	182.093	7859.102	48.077

Abbreviations: Man, mannose; Rha, rhamnose; Glu, glucose; Gal, galactose; Ara, arabinose.

Table 4 Molecular Weight and Polydispersion Index of SPS-1 and SPS-2

Sample	Mw (Da)	Mn (Da)	D
SPS-1	5546	2984	1.925
SPS-2	30902	13700	2.440

Abbreviations: Mw, Weight average; Mn, Number average molecular weight; D, Polydispersion index.

matrix which is a β-configuration glycosidic bond, which agrees with the IR spectroscopic results. The δH1.18 ppm and 1.16 ppm resonance signals in the high-field region were inferred to be a small amount of rhamnose signal peak. SPS-2 is similar to SPS-1. δH5.06 ppm belongs to the proton signal of Man, indicating that SPS-2 belongs to the α-configuration glycosidic bond. The δH1.23 ppm and δH1.16 ppm in the high-field region may be the resonance methyl proton signal peak, which is a trace of Rha signal. The maximum absorption wavelength of SPS-1 is close to that of Congo red phase, so there is no 3D helix structure, while the maximum absorption wavelength of SPS-2 shows a red shift, which is higher than that of Congo red, indicating that a complex can be formed. Thus, SPS-2 has a 3D helix structure (Figure 5D). There are absorption peaks at 3423cm^{-1}, 2924cm^{-1}, 1425cm^{-1}, 921.97cm^{-1}, and 895.45cm^{-1} indicating that SPS-1 was judged to be the residue absorption peak of β-D-man. Absorption peaks at 3423cm^{-1}, 2920cm^{-1}, 1660cm^{-1}, 1050cm^{-1}, 917cm^{-1} and 841cm^{-1} indicated that SPS-2 was α-D-galactopyranose (Figure 5E).

SPS-1 and SPS-2 can be completely reacted by KIO_4 within 2 days, and the consumption of KIO_4 and the production of formic acid are shown in Table 5. SPS-1 was mainly composed of glucans with 1→2 or 1→4 linkage glycosyl as the main chain. SPS-2 was mainly composed of 1→6 glucans bonded to the main chain. Furthermore, ara-gal with the glycosyl main chain partially bonded at the 1→3 position is present.

In the present study, we focused on the SPS-1 (subsequently replaced by SPS) fraction due to its easy access to enrich.

Table 5 Oxidation of KIO_4

Sample	Added Amount	Consumption of KIO_4	Production of CH_2O_2	Amount of Glycosyl Bonded		
				I→6	I→2/I→4	I→3
SPS-1	50	53.7	13.2	13.2	27.3	9.5
SPS-2	50	56.35	26.12	26.12	4.11	19.77

Synthesis and Characterization of the SPS-PEI Polymer

The hydrophobic moiety CDI was selected to modify the water-soluble SPS and produce the amphiphilic SPS-PEI polymer. To sum up it briefly, PEI was first created to functionally introduce *carboxyl* (-COOH), and as shown in Figure 6A, it was subsequently conjugated with SPS through an esterification reaction. The FT-IR spectra of SPS and SPS-PEI, as shown in Figure 6B, both showed a distinctive absorption band about 3400 cm^{-1}. When comparing SPS with SPS-PEI, the former revealed a characteristic deformation peak at roughly 1570 cm^{-1}, while the latter revealed a new peak at about 1700 cm^{-1}, linked to the stretching vibrations of the newly created ester carbonyl (C=O). Consequently, the synthesis of the SPS-PEI polymer was accomplished. The ^{1}H-NMR spectra for SPS-PEI, as displayed in Figure 6C, revealed additional peaks at 2.52~2.74 ppm that were attributed to the protons of PEI in addition to the distinctive SPS peaks between 3.7 and 5.3 ppm, indicating the successful attachment of PEI to SPS. By comparing the results of the monosaccharide components of SPS and SPS-PEI, the remaining complete monosaccharide components had decreased, which indicated that SPS-PEI retains some of the monosaccharide components, possibly some that were not linked (Figure 6D). The potentials of SPS before and after modification are different. After PEI modification, the potential of SPS changes, indicating that SPS-PEI carries a positive charge (Figure 6E). SPS-PEI disperses in the solution as circular or nearly circular particles, evenly dispersed, with a size of approximately 200nm nanoparticles (Figure 6F). Compared with SPS-PEI, the overall trend of both was similar before 200°C, but SPS-PEI had begun to decompose at 220°C, with a slower weight loss rate than SPS, and stabilized after 400°C, indicating that after PEI modification, its stability decreased, proving that the component of the carrier material had changed (Figure 6G). When the polymer begins to self-assemble into NPs by intra/intermolecular interaction, the threshold concentration can be used to estimate the critical aggregation concentration (CAC). The intensity ratio (I_{339}/I_{335}) of the pyrene excitation spectra as a function of the logarithm of the conjugate concentration of SPS and PEI is trended in Figure 6H. The CAC value was 6.46×10^{-3} mg/mL, which suggests that the SPS-PEI conjugate has the potential to be used as a hydrophobic drug carrier because it can self-assemble into NPs in an aqueous solution at very low concentrations and maintain the micellar structure before delivering the drug to the intended sites under extremely diluted conditions in the whole blood circulation.[16]

Synthesis and Characterization of HA-FA Polymer and siRNA-Loaded NPs

To put it succinctly, FA was first created to functionally introduce -COOH, and as Figure 7A showed, it was subsequently conjugated with HA by an esterification reaction. The FT-IR of HA-FA demonstrates that the C=O stretching vibration peak appeared at 1579 cm^{-1}. Additionally, the absorption peaks of *amino* (-NH_2) at 1640 cm^{-1} and -COOH at 3280 cm^{-1} exceeded the corresponding peak in HA (Figure 7B). The distinctive peak of FA emerged between 6.6 and 8.6 ppm, indicating that FA was successfully grafted onto HA (Figure 7C). Through electrostatic contact, the cationic NPs can form complex with siRNA. As illustrated in Figure 7D, roughly spherical NPs can be generated by combining the siRNA aqueous solution in the nuclease-free water with the blank NPs. The physiochemical characteristics of the complexes that formed were modified by adjusting the weight ratios of SPNPs, HSPNPs, and HFSPNPs to siRNA. The resulting siRNA-loaded NPs exhibit higher zeta potential as the weight ratios increase from 1:1 to 1:20, according to the DLS data in Table 6. This occurs because more cationic NPs were utilized. The weight ratio of ≥0.1 indicated a positive charge for the siRNA-loaded NPs. The proper particle size of the NPs is also important for efficient siRNA delivery.[17] When the weight ratio decreases, the siRNA-loaded NPs develop into larger particles. The 100~200 nm diameter of the positive surface-charged siRNA-loaded NPs are appropriate for cell uptake.[18,19]

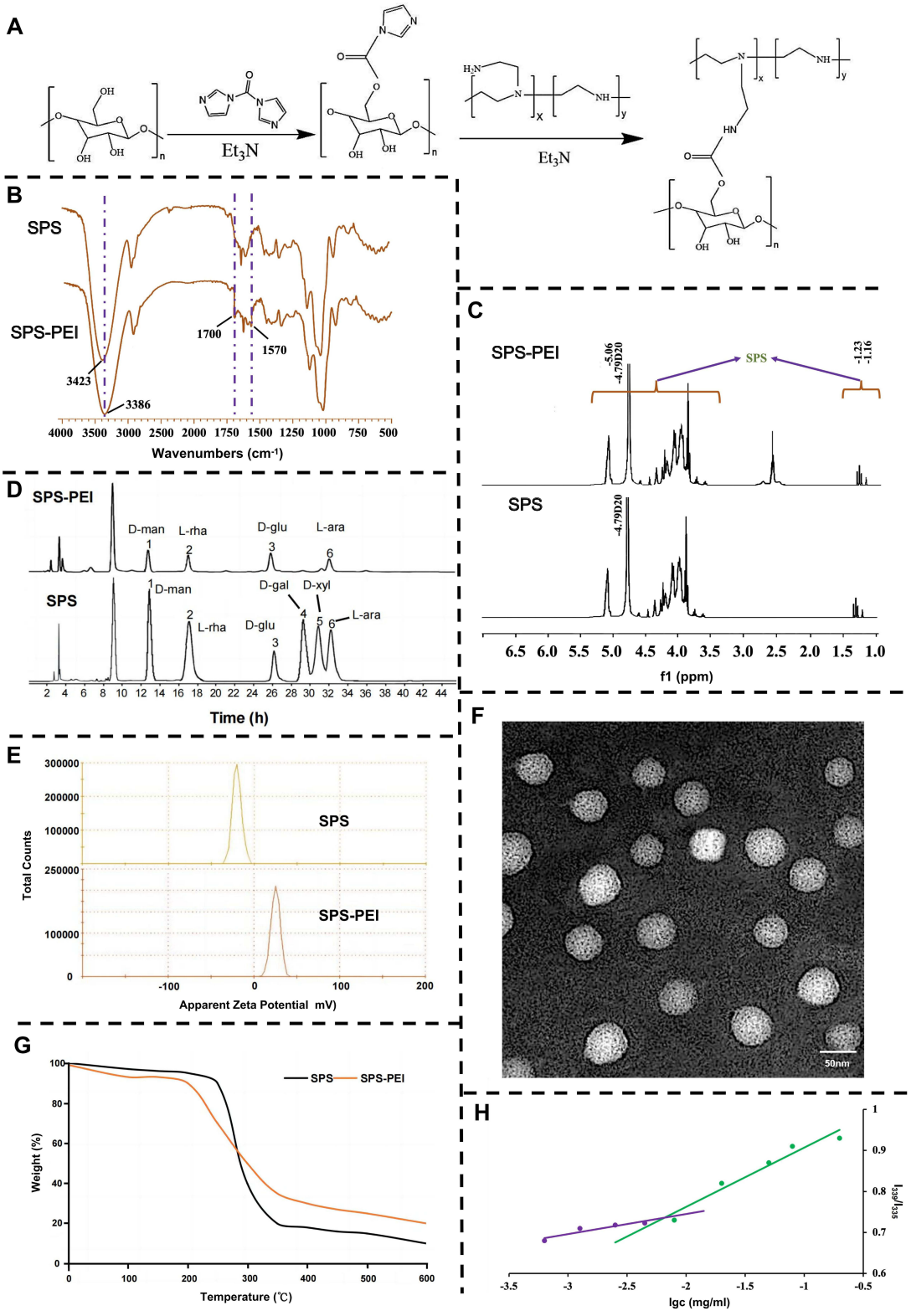

Figure 6 The synthesis process of SPS-PEI polymer (**A**). FT-IR spectrum (**B**), ^{1}H-NMR spectrum (**C**), monosaccharide composition (**D**), and zeta potential (**E**) of SPS and SPS-PEI polymer. The numbers represent the wavelengths of the corresponding peaks. TEM images of SPS-PEI polymer (**F**) (scale bar, 50 nm). Thermogravimetric analysis of SPS and SPS-PEI polymer (**G**). Critical aggregation concentration of SPS-PEI polymer (**H**).

Abbreviations: Et_3N, Triethylamine; SPS, safflower polysaccharide; PEI, polyethyleneimine; D-glu, D-glucose; D-gal, D-galactose; D-xyl, D-xylose; D-man, D-mannose; L-rha, L-rhamnose; L-ara, L-arabinose.

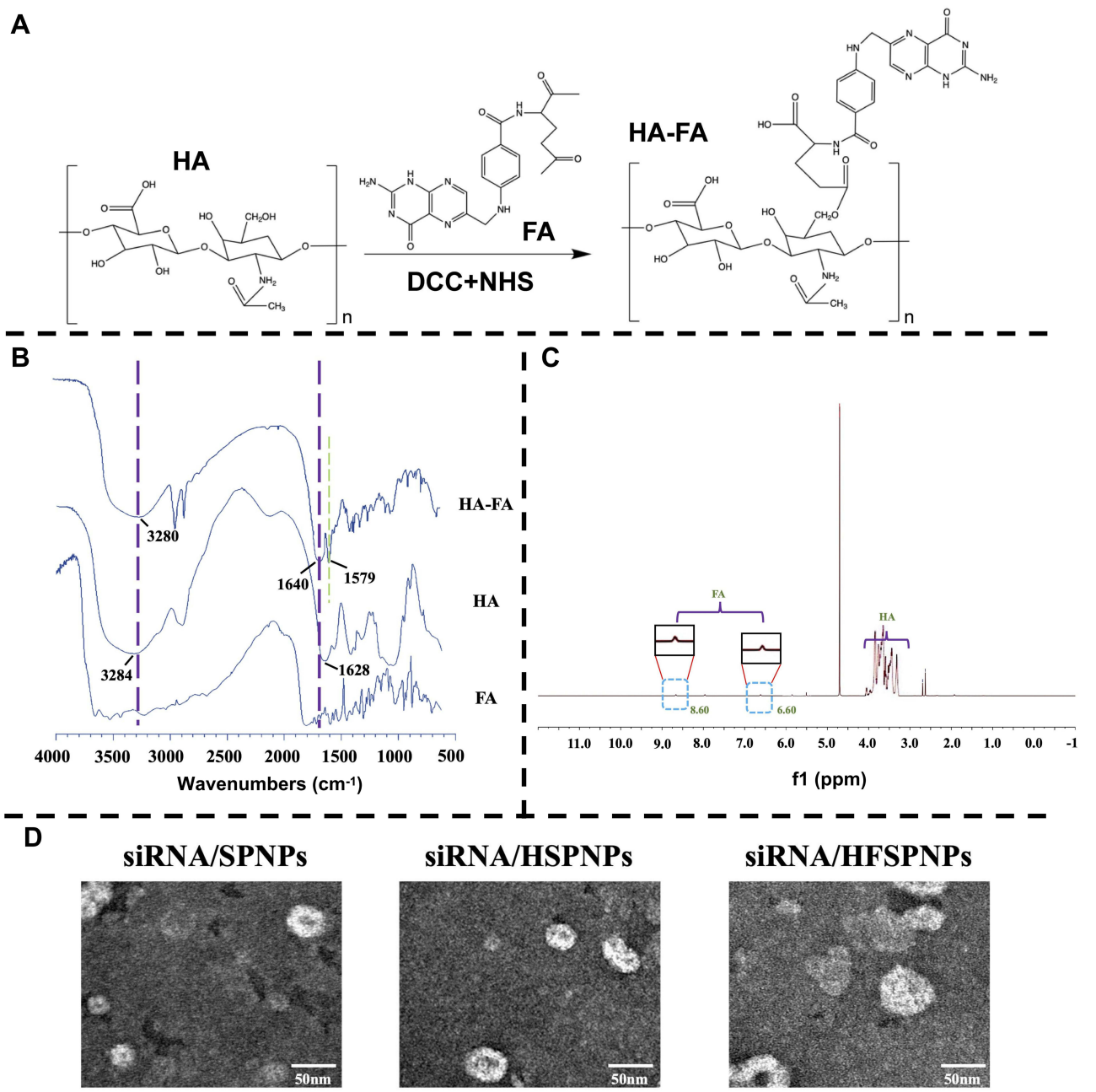

Figure 7 The synthesis process (**A**), FT-IR spectrum (**B**) and ^{1}H-NMR spectrum (**C**) of HA-FA. TEM images of siRNA-loaded NPs (**D**) (scale bar, 50 nm).
Abbreviations: DCC, Dicyclohexyl-carbodiimide; FA, Folic acid; HA, hyaluronic acid; NHS, N-butyl hydroxy; SPNPs, SPS-PEI self-assembled nanoparticles; HSPNPs, HA-SPS-PEI self-assembled nanoparticles; HFSPNPs, HA-FA-SPS-PEI self-assembled nanoparticles.

Biocompatibility of NPs

Blood biocompatibility is a crucial issue in clinical administration, particularly in intravenous administration. Uncoated SPNPs interacted with serum more over time and had a reversely high positive charge. On the other hand, following coating, there was a considerable decrease in the interaction between serum and HSPNPs and HFSPNPs, and this interaction did not change much as time passed. Time of the body for the circulation of NPs was prolonged when their binding to non-specific proteins was decreased (Figure 8A). Furthermore, through acid-base titration, the buffer capacities of NPs were determined. The results demonstrate that all of the NPs have a significantly higher proton buffering capacity than NaCl, yet when compared to HFSPNPs, SPNPs and HSPNPs have a lower buffering capacity (Figure 8B). Relatively speaking, HSPNPs and SPNPs have less amine groups than HFSPNPs, which could be one

Table 6 Characterizations of Blank NPs and siRNA-Loaded NPs

Formulation	Zeta Potential (mV)	Size (nm)	PDI	EE of siRNA (%)
SPNPs	23.17 ± 1.63	101.8 ± 9.82	0.207 ± 0.039	–
siRNA/SPNPs (1:20)	11.31 ± 1.02	132.2 ± 7.18	0.245 ± 0.028	82.5 ± 6.42
siRNA/SPNPs (1:10)	4.29 ± 0.79	141.7 ± 6.92	0.271 ± 0.019	80.9 ± 7.15
siRNA/SPNPs (1:5)	−1.76 ± 0.56	148.6 ± 6.10	0.304 ± 0.032	79.4 ± 3.82
siRNA/SPNPs (1:1)	−7.95 ± 0.94	160.8 ± 8.37	0.251 ± 0.027	67.3 ± 5.41
HSPNPs	8.44 ± 1.63	110.9 ± 9.33	0.263 ± 0.036	–
siRNA/HSPNPs (1:20)	4.02 ± 0.98	139.3 ± 5.20	0.338 ± 0.031	84.1 ± 6.10
siRNA/HSPNPs (1:10)	1.73 ± 0.31	149.2 ± 6.63	0.372 ± 0.030	79.5 ± 4.87
siRNA/HSPNPs (1:5)	−7.82 ± 0.93	157.8 ± 6.10	0.398 ± 0.041	76.2 ± 5.44
siRNA/HSPNPs (1:1)	−11.73 ± 1.27	172.2 ± 9.13	0.347 ± 0.034	62.0 ± 3.71
HFSPNPs	10.36 ± 1.73	105.3 ± 4.63	0.252 ± 0.027	–
siRNA/HFSPNPs (1:20)	4.67 ± 1.82	137.3 ± 7.10	0.319 ± 0.013	80.9 ± 4.73
siRNA/HFSPNPs (1:10)	1.98 ± 0.83	146.9 ± 8.35	0.379 ± 0.047	73.2 ± 5.02
siRNA/HFSPNPs (1:5)	−6.26 ± 0.71	155.5 ± 6.80	0.402 ± 0.020	71.0 ± 4.04
siRNA/HFSPNPs (1:1)	−10.49 ± 1.26	176.6 ± 8.23	0.351 ± 0.046	63.2 ± 3.81

Notes: Data are expressed as mean±SD. "–" indicates that there is no EE for this material.
Abbreviations: EE, encapsulation efficiencies; SPNPs, SPS-PEI self-assembled nanoparticles; HSPNPs, HA-SPS-PEI self-assembled nanoparticles; HFSPNPs, HA-FA-SPS-PEI self-assembled nanoparticles.

explanation. By using the "proton sponge" effect, HFSPNPs could boost the swelling of endocytic vesicles and transport siRNA into the cytoplasm, as demonstrated by this analysis of their strong proton buffering capacity.[20] The outstanding safety of SPNPs, HSPNPs, and HFSPNPs was demonstrated by Figure 8C and D, which showed that the cell viabilities of LO2 and SMMC-7721 cells were remained above 85% with concentrations of these blank NPs ranging from 3.1~100 μg/mL. In addition, serum stability is an essential indicator for nanocarriers. None of the NPs solution caused significant hemolysis of SD mice erythrocytes, and the hemolysis ratio was below the acceptable range (<5%) (Figure 8E).

Stability of siRNA-Loaded NPs

To estimate the storage stability of siRNA-loaded NPs, size, zeta potential, and PDI value were measured for 28 days. The average size, zeta potential, and PDI value showed no significant changes and deviations, indicating that siRNA-loaded NPs showed high stability within 28 days. In Figure 9A–C, compared with siRNA/SPNPs and siRNA/HSPNPs, the average size range of siRNA/HFSPNPs is between 135.2 nm and 147.3 nm, which showed a wider range of particle size intervals, indicating that more siRNA encapsulated in siRNA-loaded NPs. In Figure 9D–F and G–I, there were no dramatical changes in zeta potential and PDI value of siRNA-loaded NPs. The zeta potential was positive (nearly neutral), while the PDI value was all less than 0.4, indicating that siRNA-loaded NPs maintained uniformity within 28 days. The EE of siRNA decreased over time, but there was no significant difference (Figure 9J–L). These results suggested that siRNA-loaded NPs were stable in different storage and physiological condition.

In vitro Drug Release

Drug release characteristics of siRNA-loaded NPs in vitro are shown in Figure 10A. Findings showed that, after just 8 h, almost 87% of the free $siRNA^{FAM}$ was released. The release pattern of $siRNA^{FAM}$/HFSPNPs, on the other hand, was

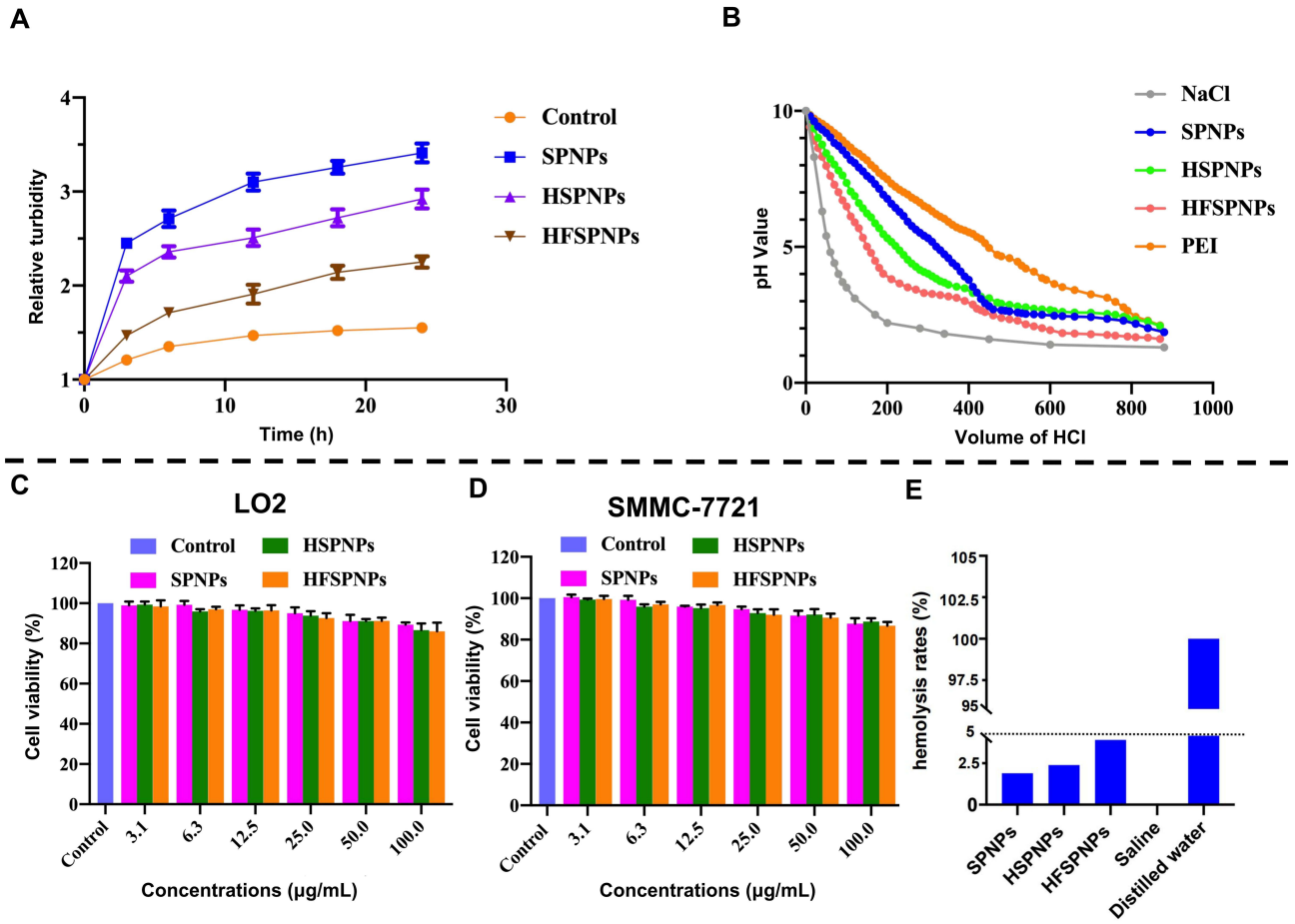

Figure 8 Serum stability (**A**) and acid-base titration (**B**) of blank NPs. Cytotoxicity analysis of NPs after incubation for 96 h on LO2 cells (**C**) and SMMC-7721 cells (**D**). Hemolysis properties of blank NPs (**E**).
Abbreviations: SPNPs, SPS-PEI self-assembled nanoparticles; HSPNPs, HA-SPS-PEI self-assembled nanoparticles; HFSPNPs, HA-FA-SPS-PEI self-assembled nanoparticles.

biphasic. A rapid release of 30% siRNA^{FAM} from HFSPNPs happened in the first 8 h, while a slow release of 54.1% took place during the next 64 h. This is most likely due to the fact that the first burst release of siRNA^{FAM} was caused by partially absorbed siRNA^{FAM} on the surface or siRNA^{FAM} entrapped close to the surface of NPs, while the sustained release was caused by the amorphous form of siRNA that was imprisoned inside HFSPNPs.[21,22] The findings suggested that HFSPNPs might find potentially relevance as a siRNA sustained release carrier.

In vitro Cellular Uptake

The cellular absorption of various siRNA^{FAM} formulations in SMMC-7721 and LO2 cells was investigated in the present work using flow cytometry and CLSM. The time-dependent cellular absorption of siRNA^{FAM}/HFSPNPs, as depicted in Figure 10B, suggested that the NPs accumulated inside cells gradually to exert their therapeutic effects. Similar results were also observed in SMMC-7721 cells. More importantly, the higher accumulation efficiency of siRNA^{FAM}/HFSPNPs compared with siRNA^{FAM}/SPNPs and siRNA^{FAM}/HSPNPs might be ascribed to the high affinity of the HFSPNPs for receptors. Furthermore, LO2 and SMMC-7721 cells presented a greater decrease in green fluorescence intensity with the prior addition of HA and FA. This was because HA (or FA) could competitively bind to and restrain the endocytosis of receptors.[23] Green fluorescence in Figure 10C and D suggested that LO2 and SMMC-7721 cells could receive siRNA^{FAM}-loaded NPs.

As predicted, after 4h of incubation with siRNA^{FAM}-loaded NPs, the green fluorescence intensities in SMMC-7721 cells were stronger than those in LO2 cells, which somewhat supports endocytosis. Quantitative flow cytometry tests were carried out to further validate the liver-targeting capacity of SPNPs, HSPNPs, and HFSPNPs. The uptake of each

https://doi.org/10.2147/IJN.S544439

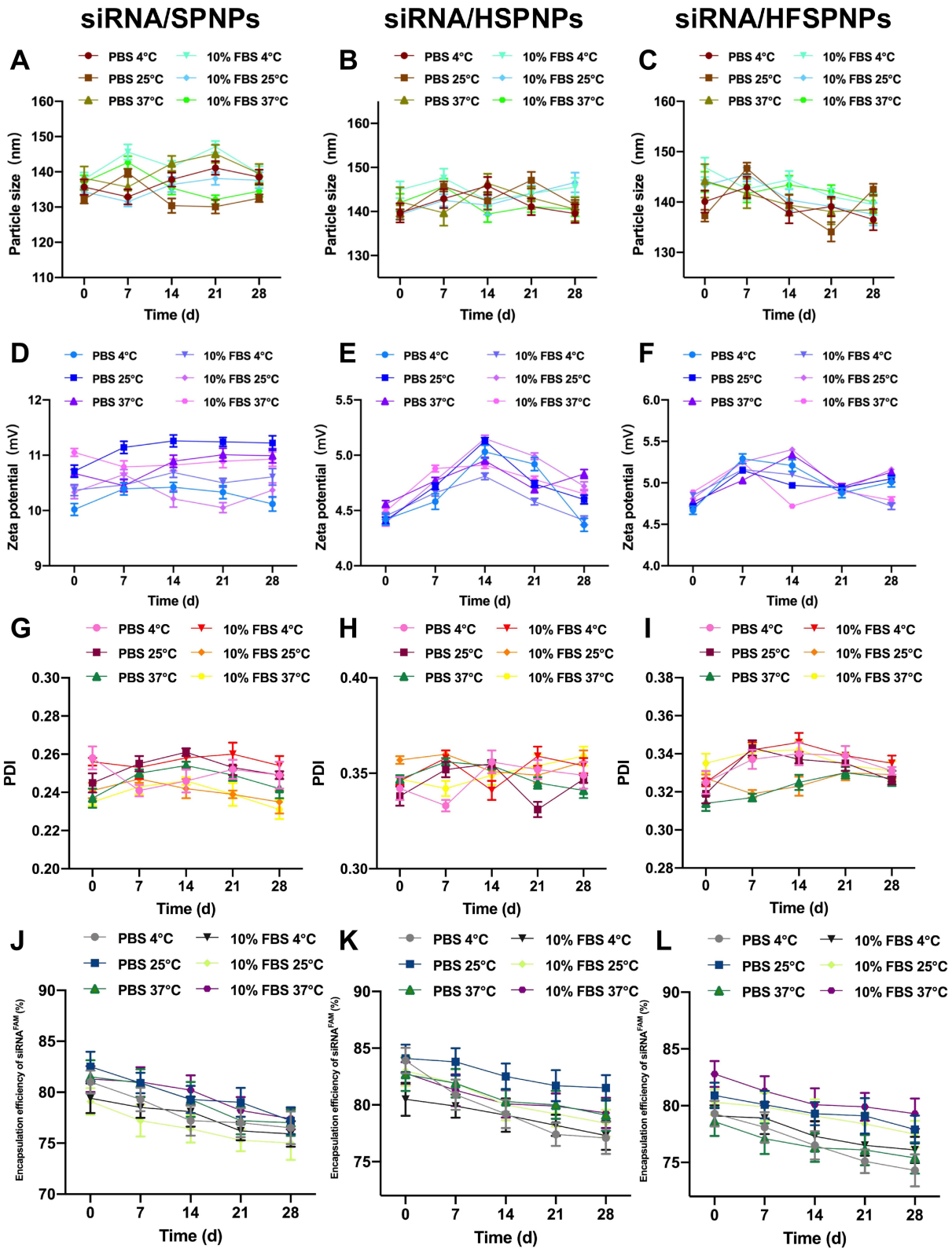

Figure 9 The particle size of siRNA/SPNPs (**A**), siRNA/HSPNPs (**B**) and siRNA/HFSPNPs (**C**) stored at different conditions for 28 days. The zeta potential of siRNA/SPNPs (**D**), siRNA/HSPNPs (**E**) and siRNA/HFSPNPs (**F**) stored at different conditions for 28 days. The PDI of siRNA/SPNPs (**G**), siRNA/HSPNPs (**H**) and siRNA/HFSPNPs (**I**) stored at different conditions for 28 days. The encapsulation efficiency of siRNA of siRNA/SPNPs (**J**), siRNA/HSPNPs (**K**) and siRNA/HFSPNPs (**L**) stored at different conditions for 28 days.

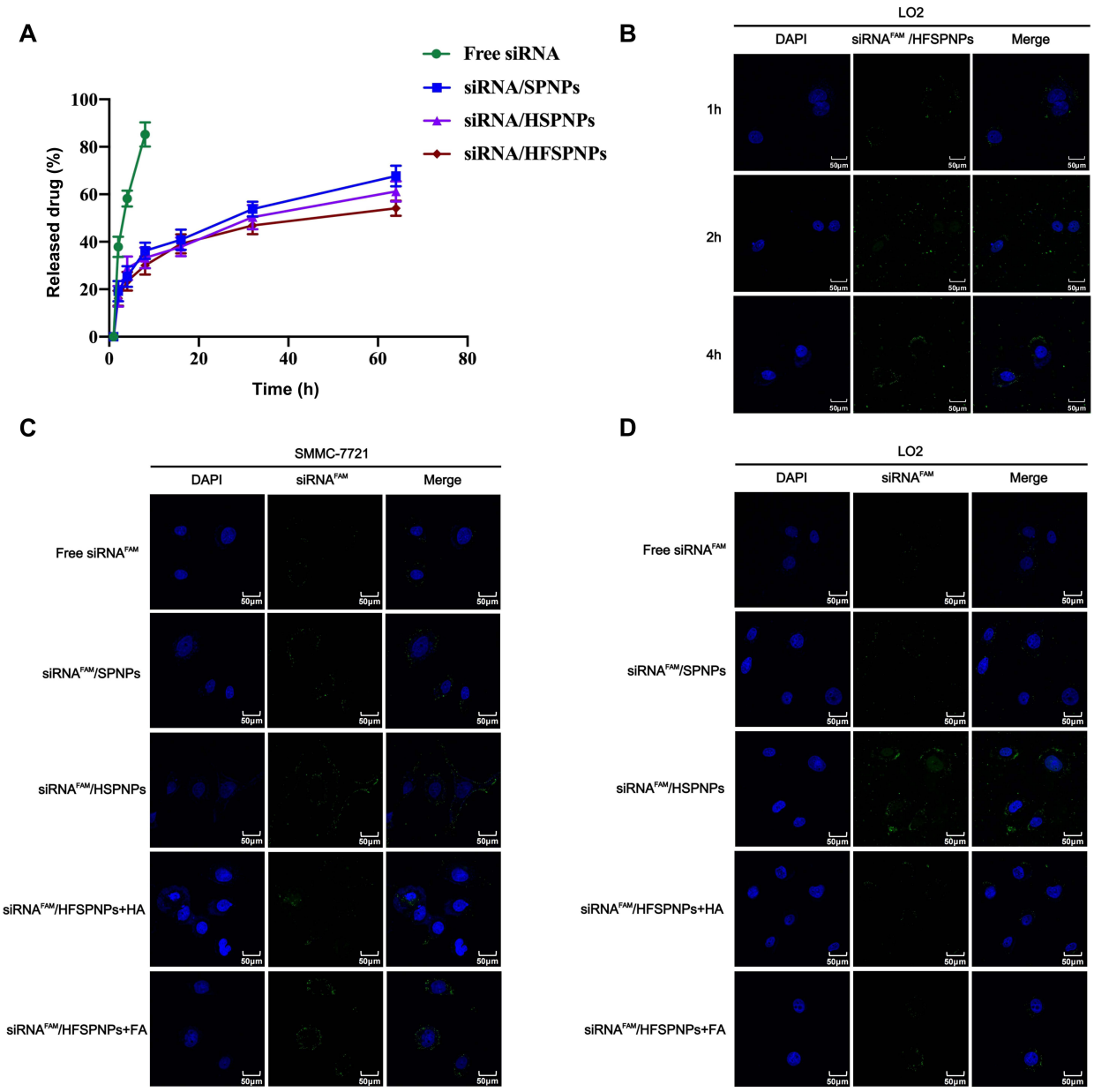

Figure 10 In vitro drug release condition of free siRNA and siRNA-loaded NPs (**A**). CLMS images of LO2 cells incubated with siRNA^{FAM}/HFSPNPs at different time points (**B**) (scale bar, 50 μm). CLMS images of SMMC-7721 cells (**C**) and SMMC-7721 cells (**D**) after 4 h treatment with different formulations (scale bar, 50 μm).
Abbreviations: SPNPs, SPS-PEI self-assembled nanoparticles; HSPNPs, HA-SPS-PEI self-assembled nanoparticles; HFSPNPs, HA-FA-SPS-PEI self-assembled nanoparticles; siRNA/SPNPs, siRNA-loaded SPNPs; siRNA/HSPNPs, siRNA-loaded HSPNPs; siRNA/HFSPNPs, siRNA-loaded HFSPNPs.

siRNA^{FAM} formulation in SMMC-7721 cells was time-dependent, as predicted, and at each time point, the mean fluorescence intensity of the siRNA^{FAM}/HFSPNPs group was significantly higher than that of the other groups (Figure 11A). The outcomes agreed with the findings by CLSM images.

In vitro Cell Apoptosis

More SMMC-7721 cells were participating in the autophagic process when treated with siBMP7/HFSPNPs as compared to cells treated with siBMP7/SPNPs and siBMP7/HSPNPs. These cells also displayed greater apoptosis and stronger red fluorescence spots. The results imply that the HA-FA coating can promote carrier uptake by SMMC-7721 cells and thus trigger the demise of cancerous cells (Figure 11B).

https://doi.org/10.2147/IJN.S544439

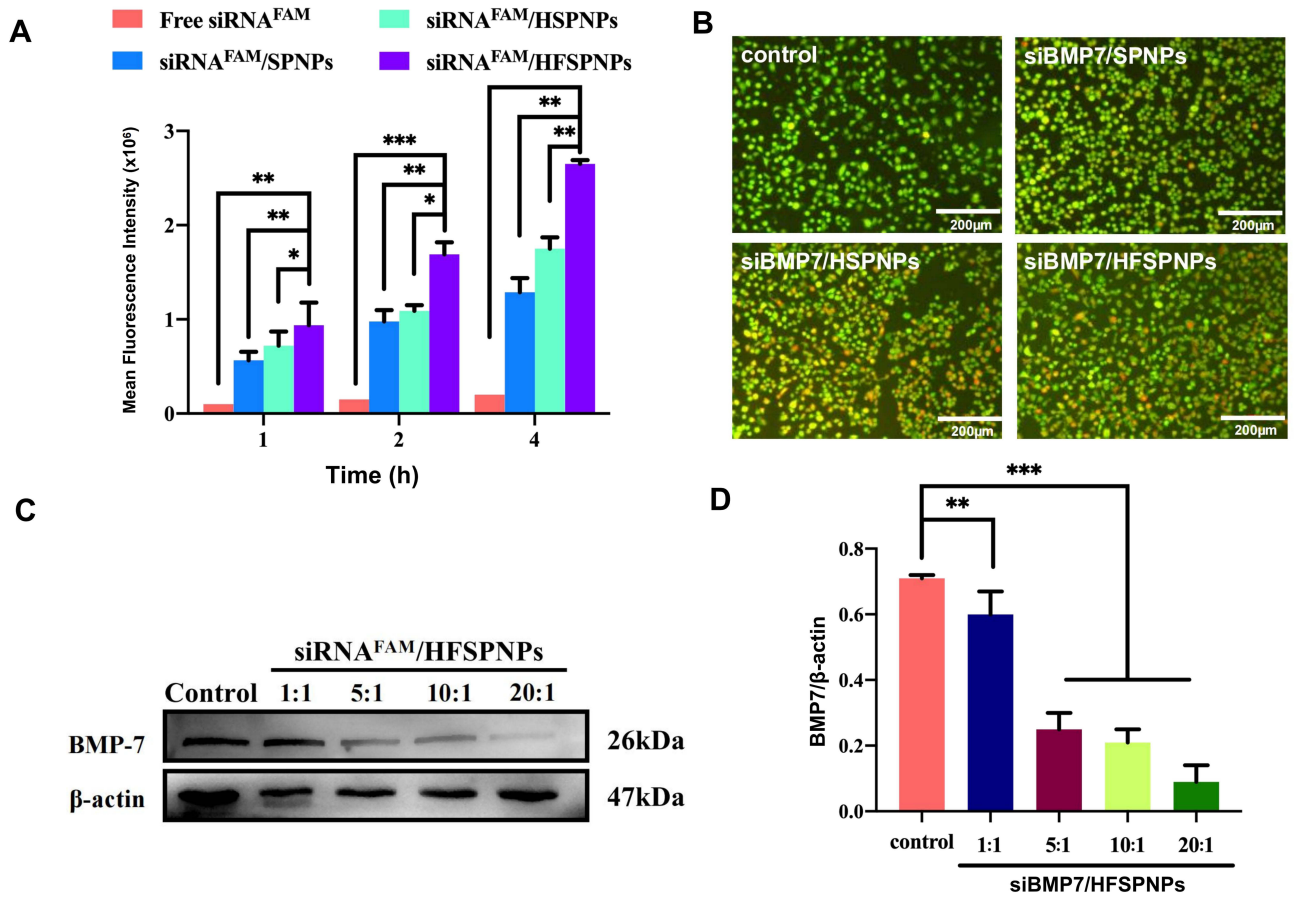

Figure 11 Quantitative flow cytometry analysis of the different formulations in SMMC-7721 cells at different time points (**A**). Data are presented as mean±SD (n=3). **P*<0.05, ***P*<0.01, ****P*<0.001 vs siRNA^{FAM}/HFSPNPs. AO staining of tumor supernatant after respective treatments (**B**) (scale bar,200 μm). Protein trace images BMP-7 (**C**) and relative molecular expression (**D**).

Abbreviations: SPNPs, SPS-PEI self-assembled nanoparticles; HSPNPs, HA-SPS-PEI self-assembled nanoparticles; HFSPNPs, HA-FA-SPS-PEI self-assembled nanoparticles; siRNA^{FAM}/SPNPs, siRNA^{FAM}-loaded SPNPs; siRNA^{FAM}/HSPNPs, siRNA^{FAM}-loaded HSPNPs; siRNA^{FAM}/HFSPNPs, siRNA^{FAM}-loaded HFSPNPs.

In vitro Transfection Efficiency

After confirming the high siRNA uptake utilizing NPs, we employed siBMP7 to assess the effectiveness of gene silencing in SMMC-7721 cells via Western blot analysis. The silencing efficacy varies were based on the weight ratios as Figure 11C and D illustrating. As the weight ratios of siBMP7 to HFSPNPs growing, more siBMP7 was internalized into the cells, resulting in a drop in BMP7 levels in the cells. In comparison to the control group, the siBMP7/HFSPNPs with a weight ratio of 20:1 could lower the BMP7 expression to about 20%.

Biodistribution

As shown in Figure 12A and B, siRNA-loaded NPs can target tumor tissues. Compared with siRNA/SPNPs and siRNA/HSPNPs, siRNA/HFSPNPs has better targeting properties. There was obvious fluorescence at the tumor site at 1 h and more NPs accumulated at the tumor site at 12 h, which indicated that the HA-FA-coated dual-targeting NPs had stronger tumor targeting properties and could deliver more siBMP7 to the tumor site to exert its therapeutic effect.

In vivo Antitumor Efficacy

Figure 12C and D showed the differences in body weights and tumor volumes. With the exception of the control group, other groups began to develop less quickly after the 7th day of formulation administration. Tumor volume remained same on day 7 but altered on day 9, while siBMP7/HFSPNPs showed total tumor inhibition before the experiment ended, indicating that treatment with siBMP7/HFSPNPs might more successfully inhibit tumor growth. Ultimately, the siBMP7/

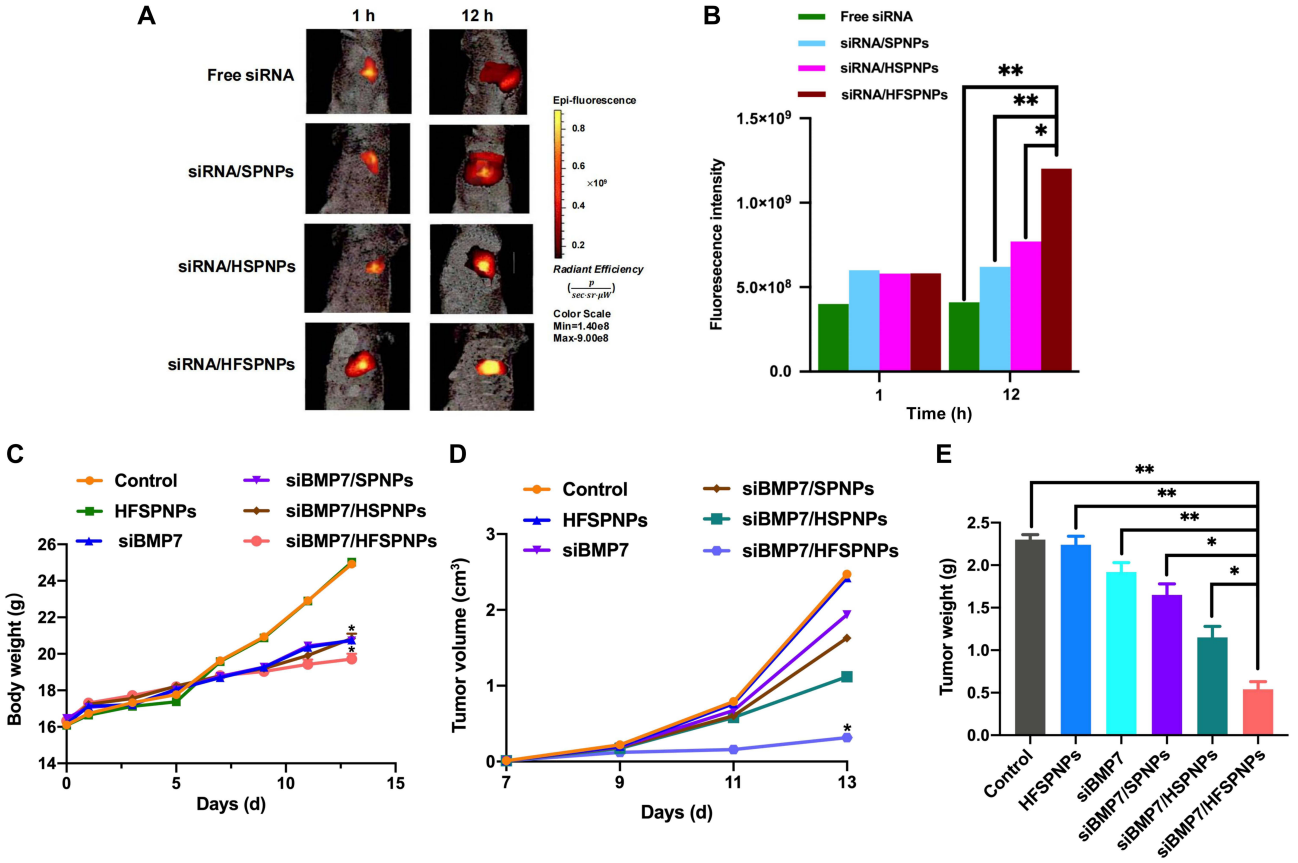

Figure 12 Whole body fluorescence images of SMMC-7721 subcutaneous xenograft mice (**A**). The corresponding average radiation efficiency of tumors in vivo (**B**). Data are presented as mean±SD (n=3). **P*<0.05, ***P*<0.01 vs siRNA^{FAM}/HFSPNPs. Changes in body weight (**C**) and tumor volume (**D**) of mice. Data are presented as mean±SD (n=3). **P*<0.05 vs control. Changes in tumor weight of mice (**E**). Data are presented as mean±SD (n=3). **P*<0.05, ***P*<0.01 vs siBMP7/HFSPNPs.

HFSPNPs inhibition rate may reach 69.5% based on the tumor quality displayed in Figure 12E. As demonstrated by H&E staining of tumor sections, different formulations reduced severe lesions, with the siBMP7/HFSPNPs group showing the largest preventative advantages (Figure 13A). Western blot might show that siBMP7/HFSPNPs could mute the BMP7 gene more successfully, enabling increased siBMP7 distribution to tumor site through Figure 13B and C.

In vivo Biosafety Evaluation

Compared with control group and HFSPNPs, siRNA-loaded NPs did not cause an increase in the expression of various factors in vivo. While siRNA did cause an increase in the expression of various factors in vivo (Figure 13D–F). It can be inferred that the HFSPNPs nanocarrier can effectively reduce the inflammatory response of siRNA in vivo which also explain the reason why siRNA causes a decrease in the weight of mice during the treatment process. In summary, siRNA/HFSPNPs could achieve an efficient and low-toxic anti-tumor effect in the anti-tumor treatment process in vivo.

As shown in Figure 14, several siRNA-loaded NPs formulations demonstrate remarkably in vivo safety. Tumor-bearing mice treated with siRNA-loaded NPs showed no significant injury to the kidney, liver, spleen, lung, or heart aside from the tumor tissue.

Discussion

Natural polysaccharides have demonstrated superior performance over other non-viral vectors in gene delivery, attributed to their ease of preparation and production, enhanced biological activity, and their capacity for hydrolysis and enzymatic degradation within cells. Moreover, natural polysaccharides possess the ability to bind to various receptors on the surface of liver cells and macrophages.[24] The breakdown products of monosaccharides and amino compounds exhibit low

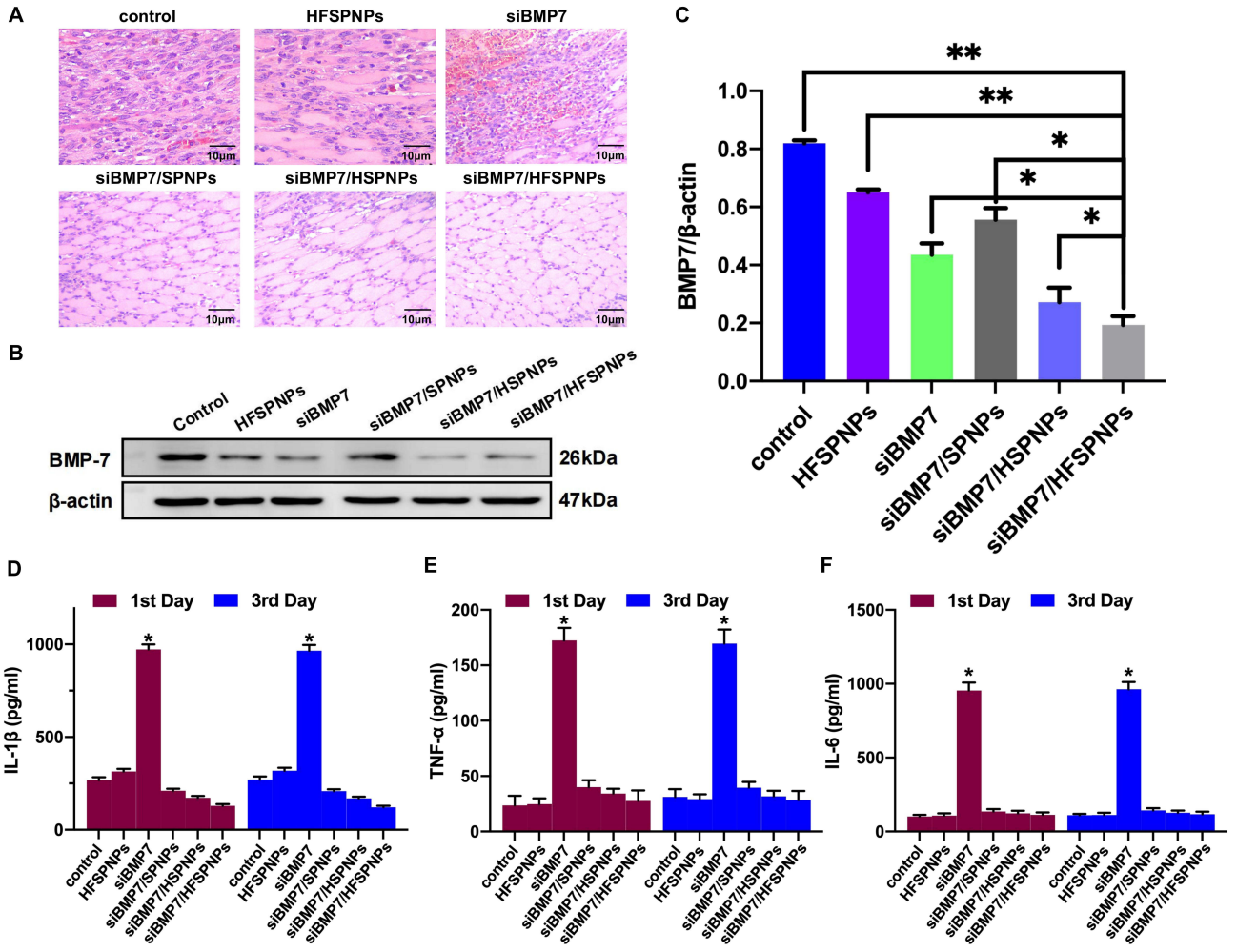

Figure 13 H&E staining of HCC tumor tissues after respective treatments (**A**) (scale bar, 10 μm). Protein trace images BMP7 (**B**) and relative molecular expression (**C**). Data are presented as mean±SD (n=3). **P*<0.05, ***P*<0.01 vs siBMP7/HFSPNPs. The inflammation level of IL-1β (**D**), TNF-α (**E**) and IL-6 (**F**) triggered by siRNA-loaded NPs. Data are presented as mean±SD (n=3). **P*<0.05 vs control.

toxicity and may even serve as nutrients, promoting cell growth. The recognition of polysaccharides by cell surface receptors can accelerate cell internalization, particularly after the design and synthesis of several naturally occurring polysaccharides through amination reactions, utilizing gene carriers with high transfection efficiency. This leads to the development of a cationic polysaccharide carrier characterized by low cytotoxicity and immunogenicity, favorable biodegradability, and high solubility in water, in contrast to those synthesized from other cationic polymers.[25] Notably, certain polysaccharides with helical structures can form hydrogen bonds with polynucleotide polymers, resulting in a hybrid three-strand helical polymer that effectively prevents polynucleotide degradation.[26] Naturally occurring polysaccharides are recognized for their low toxicity and good biocompatibility, whereas PEI, a conventional transfection reagent, is associated with a high transfection rate but significant cytotoxicity. Consequently, researchers have sought to combine the advantages of both materials by modifying natural polysaccharides with PEI as the gene carrier.[27]

HA, an acidic mucopolysaccharide, can be chemically or physically modified to create derivatives with diverse applications as materials for drug delivery vehicles.[28] HA and its derivatives are widely utilized as drug carrier materials due to their exceptional biocompatibility, biodegradability, receptor binding capabilities, non-toxicity, and low immunogenicity. Human cells exhibit a high density of HA receptors, enabling HA and its derivatives to target specific cell surface receptors for effective drug delivery. Numerous receptors are currently under investigation, including the HA receptor-1 on lymphatic endothelial cells, the CD44 receptor, the HA-mediated motility (RHAMM) receptor, and the HA endocytosis receptor.[29,30] Many tumor cells overexpress CD44 and RHAMM receptors on their surfaces, allowing HA-modified vectors to facilitate

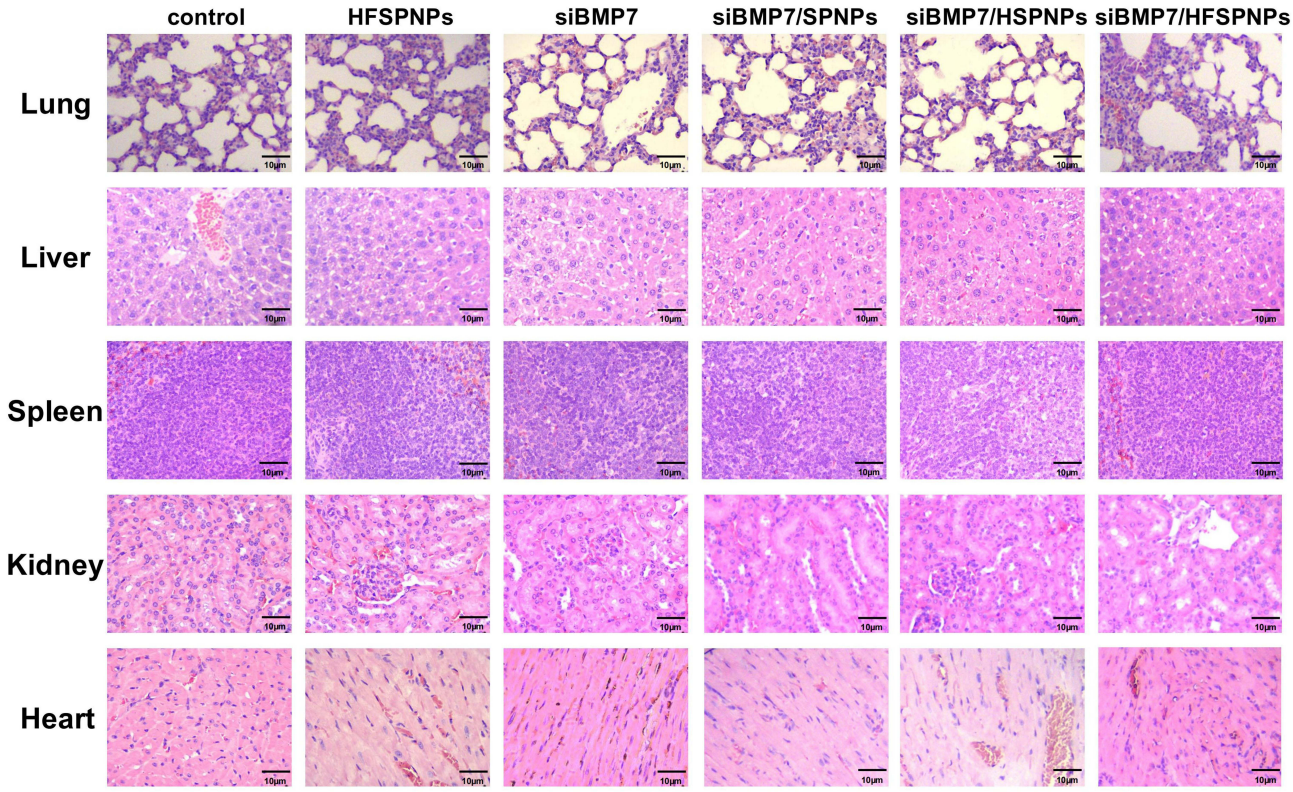

Figure 14 H&E staining of major organs after respective treatments (scale bar, 10 μm).

active targeting of drug delivery. For instance, Li et al developed an amphiphilic HA-deoxycholic acid conjugate that self-assembles into redox-sensitive micelles, specifically delivering paclitaxel into targeted cells.[31] The FA receptor, a glycoprotein, is expressed at low to moderate levels in the lungs, kidneys, and choroids, but is virtually absent from other normal tissues. In contrast, high-affinity FA receptors are significantly expressed in various malignant tumors, including ovarian, cervical, kidney, breast, and colon cancers. Folate, as a naturally occurring ligand of the FA receptor, is inexpensive, non-toxic, and readily accessible for modification. Furthermore, folate demonstrates excellent biocompatibility, robust binding to FA receptors, and minimal immunogenicity. Additionally, the folate molecule is stable and can sustain prolonged blood circulation or storage while maintaining a relatively high receptor affinity. The direct coupling of FA to drug molecules and the attachment of FA to the surface of drug carriers are the two primary methods employed by folic acid receptor-mediated active targeted drug delivery systems to direct therapeutic agents to tumor sites. Typically, the solubility of commonly utilized anti-tumor drugs is lower in aqueous environments under physiological conditions. This reduced solubility can be attributed to the direct coupling of FA to drug molecules, which further diminishes the medication's solubility in water and ultimately leads to decreased bioavailability. Consequently, the strategy of attaching FA to the surface of drug carriers holds significant research potential. At present, the FA receptor remains a central focus in the study of active targeted drug delivery systems.

To sum up, the research successfully created self-assembled NPs. HFSPNPs could effectively accumulate in hepatic cells by HA-FA-mediated uptake, according to studies done both in vitro and in vivo. This suggests that HFSPNPs could be a viable delivery mechanism for drugs to be delivered to the liver, where they might exhibit their protective effects. In SMMC-7721 cells, the siBMP7/HFSPNPs particles showed strong BMP7 knockdown along with strong in vitro and in vivo stability, strong gene loading capacity, high cell uptake, transfection efficiency, and tumor-targeting properties. Even though no harm was done to other organs, the tissue distribution staining experiment demonstrated that HFSPNPs may increase the amount of siBMP7 that accumulates in the tumor. The release of siBMP7 from the NPs allowed for the achievement of the gene therapy goal by promoting apoptosis in cancer cells and reducing the expression of BMP7

https://doi.org/10.2147/IJN.S544439

protein in tumor tissue cells. These findings suggest that HFSPNPs may be used as an HCC tumor-targeting drug in the treatment of HCC, which has implications for more research.

In summary, this research successfully developed self-assembled NPs. Studies conducted both in vitro and in vivo indicate that HFSPNPs could effectively accumulate in hepatic cells through HA-FA-mediated uptake. This finding suggests that HFSPNPs could serve as a viable delivery mechanism for drugs targeting the liver, where they may exert protective effects. In SMMC-7721 cells, the siBMP7/HFSPNPs demonstrated significant BMP7 knockdown, alongside impressive in vitro and in vivo stability, high gene loading capacity, efficient cell uptake, transfection efficiency, and tumor-targeting properties. Importantly, while no adverse effects were observed in other organs, tissue distribution staining experiments indicated that HFSPNPs may enhance the accumulation of siBMP7 in tumors. The release of siBMP7 from the NPs facilitated the achievement of gene therapy objectives by promoting apoptosis in cancer cells and reducing BMP7 protein expression in tumor tissue. These findings suggest that HFSPNPs could be utilized as a tumor-targeting drug for HCC treatment, warranting further research.

Abbreviations

MTT, 3-(4,5-dimethythiazol-2-yl)-2,5-diphenyl tetrazolium bromide; AFQ, Anti-fluorescence quenching; DCC, Dicyclohexyl-carbodiimide; FA, Folic acid; HA, hyaluronic acid; IgG, Goat anti-rabbit Immunoglobulin G; CDI, N, N-carbonyl imidazole; NHS, N-butyl hydroxy; PEI, Polyethyleneimine; TMS, Tetramethyl silane; AO, Acridine orange; HCC, Hepatocellular carcinoma; SPS, safflower polysaccharide; SPS-PEI, SPS-polyethyleneimine; HA-SPS-PEI, hyaluronic acid-SPS-polyethyleneimine; HA-FA-SPS-PEI, hyaluronic acid-folic acid-SPS-polyethyleneimine; SPNPs, SPS-PEI self-assembled nanoparticles; HSPNPs, HA-SPS-PEI self-assembled nanoparticles; HFSPNPs, HA-FA-SPS-PEI self-assembled nanoparticles; siRNA/SPNPs, siRNA-loaded SPNPs; siRNA/HSPNPs, siRNA-loaded HSPNPs; siRNA/HFSPNPs, siRNA-loaded HFSPNPs; RNAi, RNA interference; BMPs, bone morphogenetic proteins; HPLC, high performance liquid chromatography; D-glu, D-glucose; D-gal, D-galactose; D-gal-A, D-galacturonic acid; D-xyl, D-xylose; D-man, D-mannose; L-rha, L-rhamnose; L-ara, L-arabinose; PMP, pyrazolone methanol solution; GC, gas chromatography; CAC, critical aggregation concentration; PDI, polydispersity index; DAPI, 4′,6-diamidino-2-phenylindole; ppm, parts per million; RBC, red blood cells; HRs, hemolysis rates.

Data Sharing Statement

The data that support the findings of this study are available within the article and its Supplementary Material.

Ethical Approval and Informed Consent

Male BALB/c nude mice (6-weeks old, 16~20 g) (accession number: 202409100) were procured from the Experimental Animal Center of Heilongjiang University of Chinese Medicine (animal certificate: SYXK [black] 2024-103). Mice were acclimated for 1 week prior to experimentation. All studies were approved by the Institutional Animal Care and Use Committee (IACUC) of Heilongjiang University of Chinese Medicine and were conducted in accordance with the National Laboratory Animal Management Regulations and the principles of experimental animal protection.

Acknowledgments

We would like to thank Editage (www.editage.cn) for their assistance with English language editing. First authors: Haotian Bai and Jing Yang. This paper has been uploaded to ResearchSquare as a preprint: https://www.researchsquare.com/article/rs-6119667/v1.

Author Contributions

All authors made a significant contribution to the work reported, whether that is in the conception, study design, execution, acquisition of data, analysis and interpretation, or in all these areas; took part in drafting, revising or critically reviewing the article; gave final approval of the version to be published; have agreed on the journal to which the article has been submitted; and agree to be accountable for all aspects of the work.

Funding

This work was supported by the National Natural Science Foundation of China [Grant number 81603418] and Central Government Supports Local College Reform Projects under [Grant number 2020YQ05].

Disclosure

The authors report no conflicts of interest in this work.

References

1. Wan X, Yin Y, Zhou C, et al. Polysaccharides derived from Chinese medicinal herbs: a promising choice of vaccine adjuvants. *Carbohydr Polym*. 2022;276:118739. doi:10.1016/j.carbpol.2021.118739
2. Zhao G, Hong L, Liu M, et al. Isolation and characterization of natural nanoparticles in Naoluo Xintong decoction and their brain protection research. *Molecules*. 2022;27(5):1511. doi:10.3390/molecules27051511
3. Wei Z, Zhao J, Chen YM, Zhang P, Zhang Q. Self-healing polysaccharide-based hydrogels as injectable carriers for neural stem cells. *Sci Rep*. 2016;6:37841. doi:10.1038/srep37841
4. Xiong YX, Li N, Han MM, et al. Rhodiola rosea polysaccharides-based nanoparticles loaded with DOX boosts chemo-immunotherapy for triple-negative breast cancer by re-educating Tumor-associated macrophages. *Int J Biol Macromol*. 2023;239:124110. doi:10.1016/j.ijbiomac.2023.124110
5. Feng Y, Wu C, Chen H, et al. Rhubarb polysaccharide and berberine co-assembled nanoparticles ameliorate ulcerative colitis by regulating the intestinal flora. *Front Pharmacol*. 2023;14:1184183. doi:10.3389/fphar.2023.1184183
6. Ain NU, Khan B, Zhu K, et al. Fabrication of mesoporous silica nanoparticles for releasable delivery of licorice polysaccharide at the acne site in topical application. *Carbohydr Polym*. 2024;339:122250. doi:10.1016/j.carbpol.2024.122250
7. Hou X, Chen Q, Fang Y, et al. iRGD-guided silica/gold nanoparticles for efficient tumor-targeting and enhancing antitumor efficacy against breast cancer. *Int J Nanomed*. 2024;19:8237–8251. doi:10.2147/IJN.S474135
8. Zhou Z, Li M, Zhang Z, et al. Overview of Panax ginseng and its active ingredients protective mechanism on cardiovascular diseases. *J Ethnopharmacol*. 2024;334:118506. doi:10.1016/j.jep.2024.118506
9. Han MM, Fan YK, Zhang Y, Dong ZQ. Advances in herbal polysaccharides-based nano-drug delivery systems for cancer immunotherapy. *J Drug Target*. 2024;32(3):311–324. doi:10.1080/1061186X.2024.2309661
10. Robertson N, Wang P, Talebloo N, Yamada K, Moore A. Synthesis of siRNA-conjugated dextran-coated iron oxide nanoparticles for islet protection during transplantation and noninvasive imaging. *Methods Mol Biol*. 2023;2592:163–174. doi:10.1007/978-1-0716-2807-2_11
11. Al Jayoush AR, Haider M, Khan SA, Hussain Z. Hyaluronic acid-functionalized nanomedicines for CD44-receptors-mediated targeted cancer therapy: a review of selective targetability and biodistribution to tumor microenvironment. *Int J Biol Macromol*. 2025;308(Pt 2):142486. doi:10.1016/j.ijbiomac.2025.142486
12. Wang R, Li YL, Bai HT, et al. Optimization of extraction technology of safflower polysaccharide based on central composite design-response surface methodology. *JHMU*. 2022;28(05):332–338. doi:10.13210/j.cnki.jhmu.20210707.003
13. Cui D, Zhao D, Huang S. Structural characterization of a safflower polysaccharide and its promotion effect on steroid-induced osteonecrosis *in vivo*. *Carbohydr Polym*. 2020;233:115856. doi:10.1016/j.carbpol.2020.115856
14. Zhang Y, Zhang JX, Xiao LX, et al. The synergistic effect of Huangqi Gegen decoction on thrombosis relates to the astragalus polysaccharide-improved oral delivery of puerarin. *J Ethnopharmacol*. 2024;335:118622. doi:10.1016/j.jep.2024.118622
15. Liu J, Tang H, Yang L, Wang H, Li X, Yang Z. Nanophase: an effective dispersion system for the decoction of Kushen Huaihua for the treatment of ulcerative colitis. *Curr Drug Deliv*. 2025;22(6):821–836. doi:10.2174/0115672018351982250224062652
16. Zhang J, Zhang YP, Sun Q, et al. Cancer cell membrane-camouflaged pH-responsive nanoparticles for enhancing siRNA effect and synergistic anti-tumor therapy. *J Nanobiotechnology*. 2025;23(1):471. doi:10.1186/s12951-025-03508-6
17. Liu Q, Guan J, Qin L, Zhang X, Mao S. Physicochemical properties affecting the fate of nanoparticles in pulmonary drug delivery. *Drug Discov Today*. 2020;25(1):150–159. doi:10.1016/j.drudis.2019.09.023
18. Nie W, Zhang X, Kang P, et al. Exploring the influence of polysaccharide on gastrointestinal stability, drug release and formation mechanism of nanoparticles in Zhimu and Huangbai herb pair decoction. *Sci Rep*. 2025;15(1):8293. doi:10.1038/s41598-024-82130-2
19. Fu J, Liu Z, Feng Z, et al. Platycodon grandiflorum exosome-like nanoparticles: the material basis of fresh platycodon grandiflorum optimality and its mechanism in regulating acute lung injury. *J Nanobiotechnology*. 2025;23(1):270. doi:10.1186/s12951-025-03331-z
20. Patel S, Kim J, Herrera M, Mukherjee A, Kabanov AV, Sahay G. Brief update on endocytosis of nanomedicines. *Adv Drug Deliv Rev*. 2019;144:90–111. doi:10.1016/j.addr.2019.08.004
21. Sun L, Liu Y, Sun Q, et al. Polysaccharides from traditional Chinese medicine and their nano-formulated delivery systems for cancer immunotherapy. *Carbohydr Polym*. 2025;357:123416. doi:10.1016/j.carbpol.2025.123416
22. Salehiabar M, Nosrati H, Javani E, et al. Production of biological nanoparticles from bovine serum albumin as controlled release carrier for curcumin delivery. *Int J Biol Macromol*. 2018;115:83–89. doi:10.1016/j.ijbiomac.2018.04.043
23. Zhao L, Peng Y, Huang J, et al. Structural characterization of polysaccharides from Polygonatum Sibiricum and effect on alleviating hyperlipidemia in egg yolk emulsion-induced mice. *Int J Biol Macromol*. 2025;296:139808. doi:10.1016/j.ijbiomac.2025.139808
24. Zhang Y, Gu P, Wusiman A, et al. The immunoenhancement effects of polyethylenimine-modified Chinese Yam Polysaccharide-Encapsulated PLGA nanoparticles as an adjuvant. *Int J Nanomed*. 2020;15:5527–5543. doi:10.2147/IJN.S252515
25. Lin Z, Cao R, Guo X, Nie F, Xu J, Guo Y. Herbal medicine-derived natural product self-assembled nanoparticles: orchestrating chemo-chemodynamic-immunotherapy for tumor combination therapy. *Adv Healthc Mater*. 2025;14(18):e2500913. doi:10.1002/adhm.202500913
26. Mo J, Shi H, Ren K, Chen Z, Sheng X. Emerging biomedical applications of herbal extracts-based biomaterials. *Biointerphases*. 2025;20 (4):040802. doi:10.1116/6.0004748

27. Sader D, Zlotver I, Moya S, Calabrese GC, Sosnik A. Doubly self-assembled dermatan sulfate/chitosan nanoparticles for targeted siRNA delivery in cancer therapy. *J Colloid Interface Sci*. 2025;680(Pt B):763–775. doi:10.1016/j.jcis.2024.11.132
28. Dosio F, Arpicco S, Stella B, Fattal E. Hyaluronic acid for anticancer drug and nucleic acid delivery. *Adv Drug Deliv Rev*. 2016;97:204–236. doi:10.1016/j.addr.2015.11.011
29. Naghib SM, Ahmadi B, Mozafari MR. Smart physicochemical-triggered Chitosan-based nanogels for siRNA delivery and gene therapy: a focus on emerging strategies and paradigms for cancer therapy. *Curr Med Chem*. 2024;32(24):4913–4946. doi:10.2174/0109298673286052240426044945
30. Hu M, Bao J, Zhang Y, et al. Supramolecular nanoparticles of histone and hyaluronic acid for co-delivery of siRNA and photosensitizer in vitro. *Int J Mol Sci*. 2024;25(10):5424. doi:10.3390/ijms25105424
31. Shahidi M, Abazari O, Dayati P, et al. Using chitosan-stabilized, hyaluronic acid-modified selenium nanoparticles to deliver CD44-targeted *PLK1* siRNAs for treating bladder cancer. *Nanomedicine*. 2023;18(3):259–277. doi:10.2217/nnm-2022-0198